



**ornl**

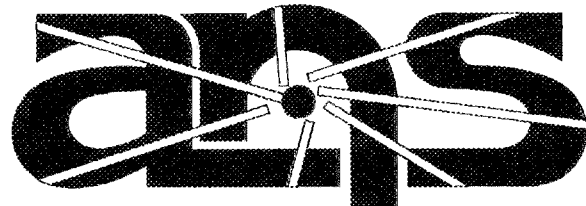
**OAK RIDGE  
NATIONAL  
LABORATORY**

**MARTIN MARIETTA**

**Follow-Up Fuel Plate Stability  
Experiments and Analyses for the  
Advanced Neutron Source**

**November 1993**

OAK RIDGE NATIONAL LABORATORY  
CENTRAL RESEARCH LIBRARY  
CIRCULATION SECTION  
4500N ROOM 115  
**LIBRARY LOAN COPY**  
DO NOT TRANSFER TO ANOTHER PERSON  
If you wish someone else to see this  
report, send in name with report and  
the library will arrange a loan.  
4007988 10 9/73



**Advanced Neutron Source**

MANAGED BY  
MARTIN MARIETTA ENERGY SYSTEMS, INC.  
FOR THE UNITED STATES  
DEPARTMENT OF ENERGY

This report has been reproduced directly from the best available copy.

Available to DOE and DOE contractors from the Office of Scientific and Technical Information, P.O. Box 62, Oak Ridge, TN 37831; prices available from (615) 576-8401, FTS 626-8401.

Available to the public from the National Technical Information Service, U.S. Department of Commerce, 5285 Port Royal Rd., Springfield, VA 22161.

This report was prepared as an account of work sponsored by an agency of the United States Government. Neither the United States Government nor any agency thereof, nor any of their employees, makes any warranty, express or implied, or assumes any legal liability or responsibility for the accuracy, completeness, or usefulness of any information, apparatus, product, or process disclosed, or represents that its use would not infringe privately owned rights. Reference herein to any specific commercial product, process, or service by trade name, trademark, manufacturer, or otherwise, does not necessarily constitute or imply its endorsement, recommendation, or favoring by the United States Government or any agency thereof. The views and opinions of authors expressed herein do not necessarily state or reflect those of the United States Government or any agency thereof.

Engineering Technology Division

**FOLLOW-UP FUEL PLATE STABILITY  
EXPERIMENTS AND ANALYSES FOR  
THE ADVANCED NEUTRON SOURCE**

W. F. Swinson  
R. L. Battiste  
C. R. Luttrell  
G. T. Yahr

November 1993

Prepared by the  
OAK RIDGE NATIONAL LABORATORY  
Oak Ridge, Tennessee 37831  
managed by  
MARTIN MARIETTA ENERGY SYSTEMS, INC.  
for the  
U.S. DEPARTMENT OF ENERGY  
under contract No. DE-AC05-84OR21400



3 4456 0379250 9



## CONTENTS

	<b>Page</b>
LIST OF FIGURES .....	v
ACRONYMS AND SYMBOLS .....	ix
ABSTRACT .....	1
1. INTRODUCTION .....	1
2. TYPE OF FLOW INVOLVED .....	3
3. DISCUSSION OF PAST WORK ON FLOW PROBLEM .....	9
4. EXPERIMENTAL ARRANGEMENT .....	15
5. DATA AND RESULTS FROM SECOND TEST OF THE ANS PLATES .....	23
6. DISCUSSION .....	53
7. CONCLUSIONS .....	57
8. REFERENCES .....	61



## LIST OF FIGURES

Figure	Page
1. Failure of the MTR fuel plates . . . . .	10
2. Conceptual core design. . . . .	16
3. Plate arrangement in support cylinders . . . . .	17
4. Flow test loop . . . . .	18
5. Flow straightener for the lower element . . . . .	19
6. Lower plate test element . . . . .	20
7. Plate calibration arrangement . . . . .	21
8. Channel pressure drop vs velocity, second model upper ANS plates, all channels . . . . .	26
9. Channel pressure drop vs velocity, second model upper ANS plates, Channel A9-A4 . . . . .	26
10. Channel pressure drop vs velocity, second model upper ANS plates, Channel A4-A8 . . . . .	27
11. Channel pressure drop vs velocity, second model upper ANS plates, Channel A8-A1 . . . . .	27
12. Channel pressure drop vs velocity, second model upper ANS plates, Channel A1-A5 . . . . .	28
13. Channel pressure drop vs velocity, second model lower ANS plates, all channels . . . . .	28
14. Channel pressure drop vs velocity, second model lower ANS plates, Channel B15-B18 . . . . .	29
15. Channel pressure drop vs velocity, second model lower ANS plates, Channel B4-B15 . . . . .	29
16. Channel pressure drop vs velocity, second model lower ANS plates, Channel B14-B4 . . . . .	30
17. Channel pressure drop vs velocity, second model lower ANS plates, Channel B6-B14 . . . . .	30
18. Plate A1, A8, A4 entrance deflection, second model upper ANS plates . . . . .	31
19. Plate A1, A8, A4 quarter point deflection, second model upper ANS plates . . . . .	31
20. Plate A1, A8, A4 half point deflection, second model upper ANS plates . . . . .	32

21.	Plate A1, A8, A4 three-quarter point deflection, second model upper ANS plates . . . . .	32
22.	Plate A1, A8, A4 exit deflection, second model upper ANS plates . . . . .	33
23.	Plate B14, B4, B15 entrance deflection, second model lower ANS plates . . . .	33
24.	Plate B14, B4, B15 quarter point deflection, second model lower ANS plates .	34
25.	Plate B14, B4, B15 half point deflection, second model lower ANS plates . . .	34
26.	Plate B14, B4, B15 three-quarter point deflection, second model lower ANS plates . . . . .	35
27.	Plate B14, B4, B15 exit deflection, second model lower ANS plates . . . . .	35
28.	Upper element plate A1 vs position on plate at different prototype velocities, second test on upper element . . . . .	36
29.	Upper element plate A8 vs position on plate at different prototype velocities, second test on upper element . . . . .	36
30.	Upper element plate A4 vs position on plate at different prototype velocities, second test on upper element . . . . .	37
31.	Lower element plate B14 vs position on plate at different prototype velocities, second test on lower element . . . . .	37
32.	Lower element plate B4 vs position on plate at different prototype velocities, second test on lower element . . . . .	38
33.	Lower element plate B15 vs position on plate at different prototype velocities, second test on lower element . . . . .	38
34.	Plate A1, A8, A4 entrance pressure differential, second model upper ANS plates . . . . .	39
35.	Plate A1, A8, A4 quarter point pressure differential, second model upper ANS plates . . . . .	39
36.	Plate A1, A8, A4 half point pressure differential, second model upper ANS plates . . . . .	40
37.	Plate A1, A8, A4 three-quarter point pressure differential, second model upper ANS plates . . . . .	40
38.	Plate A1, A8, A4 exit point pressure differential, second model upper ANS plates . . . . .	41
39.	Plate B14, B4, B15 entrance pressure differential, second model lower ANS plates . . . . .	41
40.	Plate B14, B4, B15 quarter point pressure differential, second model lower ANS plates . . . . .	42
41.	Plate B14, B4, B15 half point pressure differential, second model lower ANS plates . . . . .	42

42.	Plate B14, B4, B15 three-quarter point pressure differential, second model lower ANS plates . . . . .	43
43.	Plate B14, B4, B15 exit pressure differential, second model lower ANS plates . . . . .	43
44.	Plate A1, A8, A4 entrance dynamic pressure, second model upper ANS plates . . . . .	44
45.	Plate A1, A8, A4 quarter point dynamic pressure, second model upper ANS plates . . . . .	44
46.	Plate A1, A8, A4 half point dynamic pressure, second model upper ANS plates . . . . .	45
47.	Plate A1, A8, A4 three-quarter point dynamic pressure, second model upper ANS plates . . . . .	45
48.	Plate A1, A8, A4 exit point dynamic pressure, second model upper ANS plates . . . . .	46
49.	Plate B14, B4, B15 entrance dynamic pressure, second model lower ANS plates . . . . .	46
50.	Plate B14, B4, B15 quarter point dynamic pressure, second model lower ANS plates . . . . .	47
51.	Plate B14, B4, B15 half point dynamic pressure, second model lower ANS plates . . . . .	47
52.	Plate B14, B4, B15 three-quarter point dynamic pressure, second model lower ANS plates . . . . .	48
53.	Plate B14, B4, B15 exit point dynamic pressure, second model lower ANS plates . . . . .	48
54.	Plate A4 entrance gage response vs time, flow velocity 33.4 m/s . . . . .	49
55.	Plate B4 entrance gage response vs time, flow velocity 23.5 m/s . . . . .	49
56.	Lower plate deflection at three-quarter section for comparison of all plates from both test elements . . . . .	50
57.	Lower plate deflection at entrance section for comparison of all plates from both test elements . . . . .	50
58.	Upper plate deflection at three-quarter section for comparison of all plates from both test elements . . . . .	51
59.	Upper plate deflection at entrance section for comparison of all plates from both test elements . . . . .	51



## ACRONYMS AND SYMBOLS

ANS	Advanced Neutron Source
HFIR	High Flux Isotope Reactor
ILL	Institut Laue-Langevin
ETR	Engineering Test Reactor
MTR	Materials Test Reactor
$A, A_{FS}$	cross-sectional flow area, cross-sectional area of flow straightener, respectively
$D$	hydraulic diameter
$b$	flow channel width
$f$	friction coefficient of resistance
$g_c$	dimensional constant
$h$	flow channel height
$L$	length of flow path
$\Delta p, \Delta p_L$	pressure difference across a plate, pressure drop along a channel length, respectively
$P_w$	wetted perimeter
$Q_p, Q_m$	prototype, model flow volume, respectively
$R_e$	Reynolds' number
$u$	flow velocity along x-coordinate
$v, v_m$	flow velocity, model flow velocity, respectively
$v_{FSM}, v_s$	flow velocity in model flow straightener, friction velocity, respectively
$w$	flow velocity along z-coordinate
$\delta_1, \delta$	laminar sublayer, boundary layer, respectively
$\mu$	fluid viscosity
$\nu$	kinematic viscosity
$\rho$	fluid density
$\tau$	shear stress



# **FOLLOW-UP FUEL PLATE STABILITY EXPERIMENTS AND ANALYSES FOR THE ADVANCED NEUTRON SOURCE**

W. F. Swinson  
R. L. Battiste  
C. R. Luttrell  
G. T. Yahr

## **ABSTRACT**

The reactor for the planned Advanced Neutron Source uses closely spaced plates cooled by heavy water flowing through narrow channels. Two sets of tests were performed on the upper and lower fuel plates for the structural response of the fuel plates to the required high coolant flow velocities. This report contains the data from the second round of tests. Results and conclusions from all of the tests are also included in this report. The tests were done using light water on full-scale epoxy models, and through model theory, the results were related to the prototype plates, which are aluminum-clad aluminum/uranium silicide involute-shaped plates.

---

## **1. INTRODUCTION**

A second round of flow experiments has been carried out on epoxy full-scale models of the upper and lower Advanced Neutron Source (ANS) fuel plates. The tests were performed to give a broader data base for drawing conclusions and to help gain confidence in the results by demonstrating repeatability. The data from these tests are illustrated in this report, which is a follow-up to the earlier work reported in ORNL/TM-12353.<sup>1</sup> The reader should refer to the earlier report for a description of the plates and the flow loop. Conclusions drawn from the second round tests are noted in this report. In addition, to help assess the structural response of the ANS fuel plates to flow, a review of earlier tests by other investigators on stability of flat plates, and of problems identified in beginning operation of the Engineering Test Reactor (ETR) plates, the Materials Test Reactor (MTR) plates, and the High Flux Isotope Reactor (HFIR) plates, are discussed. Some complications of finding analytical solutions for this complicated turbulent flow problem are noted. The potential of using the dynamic pressure as a conservative but functional design parameter is noted.



## 2. TYPE OF FLOW INVOLVED

As a first step in trying to correlate all of the flow tests that have been done (flat plates, ETR, MTR, HFIR, and ANS), the type of flow in the coolant channels is examined. Where appropriate, this examination is based on the ANS experimental flow loop, which has a flow straightener followed by a plate section containing six flow channels and five plates. As a specific reference velocity where needed, the initial planned ANS operating velocity of 27.4 m/s (89.9 ft/s) has been used. After the data for this section of the report were compiled, the planned ANS operating flow velocity was changed from 27.4 m/s to 25 m/s.

The prototype volume flow is calculated as

$$Q_p = Av = 14.7 \text{ l/s (232.6 gpm)} \quad , \quad (1)$$

where  $A$  is the cross-sectional flow area and  $v$  is the flow velocity. The model flow volume and velocity in the flow loop are

$$\begin{aligned} Q_m &= 3.0 \text{ l/s (48.0 gpm)} \quad , \\ v_m &= 5.66 \text{ m/s (18.56 fps)} \quad . \end{aligned} \quad (2)$$

The type of flow in the flow straightener is turbulent. This is apparent as flow between infinite parallel plates is turbulent if the Reynolds' number is greater than 1400. In the flow straightener, Reynolds' number is 42,557 where the boundaries are taken as parallel plates. In addition, turbulent flow is predicted when approximating the flow cross section as circular using the hydraulic diameter analogy

$$\begin{aligned} A_{FS} &= 981.9 \text{ mm}^2 \quad , \\ D &= 4 A_{FS} / P_w = 23.3 \text{ mm (.918 in.)} \quad , \end{aligned} \quad (3)$$

where  $P_w$  is the wetted perimeter,  $A_{FS}$  is the flow straightener cross-sectional area, and  $D$  is the hydraulic diameter. The flow straightener has a velocity of

$$v_{FSM} = 3084.8 \text{ mm/s (121.449 in./s)} ; \quad (4)$$

thus, the Reynolds' number is

$$R_e = v_{FSM} D / \nu = 71002 , \quad (5)$$

where  $\nu$  is the kinematic viscosity.

This Reynolds' number places the flow well into the turbulent range.

The type of flow in a typical flow channel is also turbulent. In this case, Reynolds' number is 7043, and, when compared to a turbulent Reynolds' number of 1400 for parallel plates, suggests highly turbulent flow. Turbulent flow is also predicted by approximating the flow cross section as circular using the hydraulic diameter analogy

$$D = 2.50 \text{ mm (0.0982 in.)} , \quad (6)$$

and Reynolds' number is  $R_e = 13934$ . Again, the Reynolds' number places the flow into the turbulent range.

The assumption of using the hydraulic diameter to approximate an involute cross section as a circle raises questions as to whether or not this is reasonable. This approach was used in estimating the pressure loss in HFIR and found to be reasonable. Using this same concept, the calculated pressure loss is compared with the measured pressure loss in the test loop.

$$\Delta p_L = \frac{f L \rho v^2}{2D} \quad (7)$$

is the pressure drop equation usually listed for pipes,

where

$f$  = the friction coefficient of resistance,

$L$  = flow path length,

$\rho$  = mass density of fluid,

$v$  = flow velocity,

$D$  = pipe diameter.

The coefficient of resistance can be expressed from the Blasius' formula for smooth pipes as

$$f = 0.316/R_e^{1/4} \quad . \quad (8)$$

Therefore, the pressure loss can be calculated as

$$\Delta p_L = \frac{0.158L}{g_c^{0.75} D^{1.25}} \mu^{0.25} \rho^{0.75} v^{1.75} \quad .$$

As an example, the pressure loss in the flow loop using the model ANS operating velocity (5.656 m/s) is calculated as

$$\Delta p_L = 98109 \text{ Pa (14.23 psi)} \quad . \quad (10)$$

Comparing this value to the experimental value of

$$\Delta p_L = 97447 \text{ Pa (14.13 psi)} \quad , \quad (11)$$

it can be seen that the values are very close to the same. This comparison does suggest that in calculating "overall" flow values such as pressure losses and average flow velocities, the hydraulic diameter analogy is helpful. However, it would be a mistake to assume that because the overall result is reasonable, local effects such as buckling instabilities can also be calculated with a similar analogy. The overall effect is not too surprising in that a free body shows that for fully developed turbulent flow

$$\Delta p_L (b) (h) = \tau L (b + h)^2 \quad , \quad (12)$$

and since  $h \ll b$  ,

$$\tau \approx \Delta p_L h / 2L \quad . \quad (13)$$

From the pipe analogy,

$$\tau = (\Delta p_L / 2L) (D/2) \quad . \quad (14)$$

Thus, the two equations are essentially the same when it is observed that

$$D/2 = 1.24 \text{ mm} \quad (15)$$

and compares favorably with  $h = 1.27 \text{ mm}$ . By substituting the pressure loss into the above equation, the shear stress can be calculated as

$$\tau = 0.0395 \mu^{0.25} \rho^{0.75} \frac{v^{1.75}}{g_c^{0.75} D^{0.25}} \quad . \quad (16)$$

The flow in the channels is highly turbulent flow and essentially occurs throughout the channel length. A term called friction velocity<sup>2</sup> is defined as

$$v_* = (|\tau|/\rho)^{1/2} \quad . \quad (17)$$

The laminar sublayer of the boundary layer is estimated as

$$\delta_1 = 5\nu/v_* = 0.015 \text{ mm} \quad . \quad (18)$$

To appreciate that the flow is turbulent essentially throughout its length, consider the boundary layer development over a flat plate as

$$\delta = 0.37x^{4/5}(v/\nu)^{-1/5} \quad . \quad (19)$$

For the boundary layer to develop to half of a channel thickness requires a distance of

$$x = 16.99 \text{ mm} \quad (20)$$

Thus, it is believed that the flow in the channels is highly turbulent essentially over the entire length of the plate and that it has a very thin laminar sublayer.

Having an analytical solution to this turbulent flow problem would be most desirable. To appreciate what an analytical solution would have to describe, one should examine some of the basic concepts included in turbulent flow. The flow is not a continuum, but it is composed of a complicated set of varying swirls and eddies. Thus, in some cases (probably in this case), an analytical solution should account for these temporal swirls and eddies that have strong effects at local boundaries. The swirls and eddies continually change and thus transport momenta continuously in and out of a control volume. As a result of this, the velocity and pressure are subject to continuous variation. Schlichting<sup>2</sup> notes "lumps of fluid" fluctuate in the flow direction and at right angles to the flow direction. This type of flow behavior may not lend itself to a continuum model. An attempt to describe this action is suggestive of a "mean motion" and a "fluctuation" or "eddy motion," where the velocity components and pressure are expressed as

$$u = \bar{u} + u' , v = \bar{v} + v' , w = \bar{w} + w' , p = \bar{p} + p' , \quad (21)$$

with the prime denoting change with respect to time. These terms give rise to fluctuating normal stresses as well as fluctuating shear stresses. Not having a relation for this temporal fluctuation puts an extreme limitation on finding an analytical solution to some fluid flow problems. The temporal phenomenon can be included in the equations of motion (Navier-Stokes equations); however, one can see that in addition to not having a functional relation for the fluctuations, the boundary conditions connecting a point inside an eddy zone to one just outside are unknown. Rouse<sup>3</sup> says in regard to these types of turbulent flow problems, "However correctly the Navier-Stokes equations may describe conditions at any point at any instant, it is obviously futile to attempt to use them in investigating a finite portion of the flow for a finite length of time—unless it is found possible so to modify them that the complexity of the secondary fluctuations will not conceal the basic essentials of the

flow.” Experiments are needed to tell which turbulent flow problems can be adequately modeled as a continuum and which cannot.

### 3. DISCUSSION OF PAST WORK ON FLOW PROBLEM

An early problem detected in reactor design had to do with failure of the fuel plates because of coolant flow. Stromquist and Sisman<sup>4</sup> reported on some work they did with fuel plate assemblies subjected to flow. Relative to so-called plate buckling, they concluded, "Buckling of plates can occur only under very unusual conditions, such as a combination of improper plate spacing, insufficient restraint of plate ends, and brazing defects. Calculations indicate that improper spacing alone cannot cause pressure differences as great as those shown by static pressure tests to be necessary for buckling." Improper plate spacing meant very large differences, e.g., 15.9-mm channel thickness on one side of the outside plate and 3-mm channel thickness on the other side of the outside plate. Problems with attaching the plates to the side supports accounted for other failures. It appears that the outside plates where spacing was different on each side of the plates were most susceptible to deflection problems. It should be noted that what is called "buckling" in this investigation was not buckling as in unstable structures but deflection because of load (pressure). This is apparent when it is appreciated that a flat plate fixed on two opposite boundaries and loaded transversely does not buckle because the membrane load is always tension.

In the late 1950s, some plate problems associated with the ETR were investigated and reported in Doan,<sup>5</sup> Beck et al.,<sup>6</sup> and Beck.<sup>7</sup> Some plate failures were noted with the flat plates subjected to flow. It appears that the problems were not buckling because of flow but were initiated by brazing the plates to the support sides. The brazing not only introduced residual stresses but also reduced the yield stress property of the plates. This was evident in that the plates were not flat, and the spacings between plates were irregular. The representative failed plates that were pictured appeared more like a sine wave with respect to the length of the plate than a bow with maximum deflection at the center. When different techniques for attaching the plates to the side supports were used, the failures stopped with one exception. The exception was a single case with plates attached using the new techniques but with slightly bowed plates after testing. When the dynamic pressure from the test velocity was applied to the plates, the maximum stress calculated equaled the yield stress. It does appear that if the problems pointed out by Stromquist and Sisman<sup>4</sup> had been fully appreciated, some of the problems with the ETR plates could have been avoided.

Bartz and Francis<sup>8</sup> reported on problems with the fuel plates of the MTR. This reactor had curved plates instead of flat plates as in the ETR and thus a more rigid plate. The reactor functioned for two years, during which time the plate design was changed, before any plate failures were found. The problems seemed to occur with the outside plates. The outside plates were peculiar in that the outside channel of the outside plate was different in comparison to the inside channel of the outside plate. The failure that was discussed occurred as shown in Fig. 1. The failed plate was bounded by one channel that had a pressure related to the fluid friction in that channel. The other channel bounding the failed plate had a pressure related to the channel flow and also to the pressure on the outside of the support sides because of the gap between element B and element A. This could cause a large pressure differential across the plate and initiate failure. The differential pressure across a plate was reported as 6894 Pa during the initial two years of operation. With the design changes, the differential pressure went up to 71013 Pa, and the result was plate failures. In 1954, with further and final design changes, the differential pressure dropped to 15168 Pa, and no further failures were experienced.

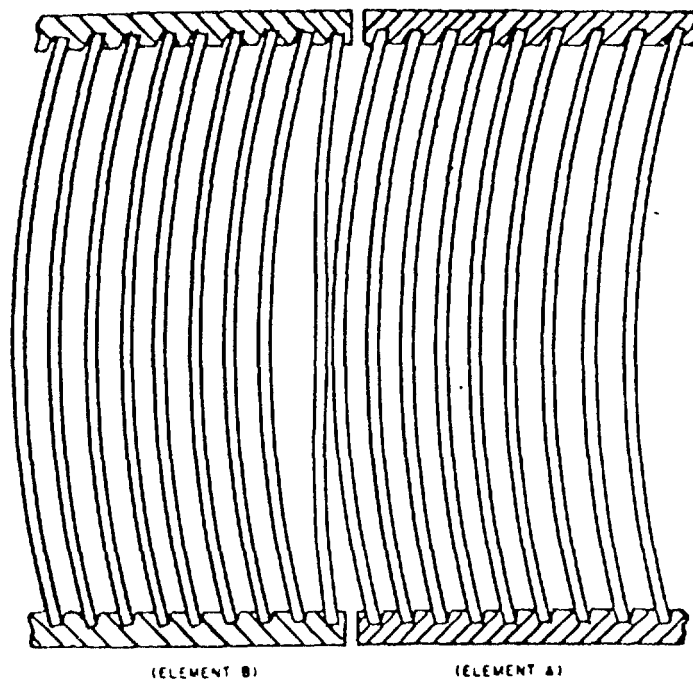


**Fig. 1. Failure of the MTR fuel plates.**

Miller<sup>9</sup> published an analytical model to describe so-called collapse of parallel-plate fuel assemblies. No experimental evidence was presented to support this theory. In comparing this theory with flat plate experiments done later in the 1960s, no correlation could be established. The assumptions made in developing this theory are difficult to justify with real flow systems. For example, applying Bernoulli's theorem to turbulent flow is not correct. The most difficult assumption to justify is assuming constant mass flow in each channel regardless of whether the channel becomes large or small during the flow process. Other complications, such as not considering how membrane stress affects the deflection, are present. Miller suggested that the problems associated with the ETR fuel plates lent some support to his theory. This is difficult to appreciate when the problems associated with the ETR plates were because of techniques of attaching the plates to the side supports.<sup>5-7</sup> Further, the mode of failure for the ETR plates was not at all like the mode of failure predicted with Miller's model. Finally, the problems associated with the ETR plates occurred at about half the velocity predicted by Miller's model. This failure would suggest that the problem was something other than the Miller collapse velocity.

Zabriskie<sup>10</sup> reported on experimental data from flat plates associated with this flow problem. Test runs included single and multiple plates made of aluminum and plexiglass with different channel and plate thicknesses. Zabriskie noted considerable scatter in the test data. The absence of sudden collapse of the channel, as predicted by the Miller model, was notable. Since no collapse was observed, a new use of the term collapse was defined. The definition used said that any observable motion of the plates was taken as the initiation of collapse, a rather imprecise use of the term. It appears from Simon<sup>11</sup> that this observable plate motion was 0.051 mm with a channel width of 2.54 mm. The deflection data was not measured and was called "apparent deflection." In trying to come up with a specific velocity to call a collapse velocity, the criteria used were when the difference in total pressure across the plate at the exit changed signs. Zabriskie observed that the plates had a small oscillation at certain velocities that would cause a change in the sign of total exit pressure difference. It seems unreasonable to correlate the Miller collapse model with this kind of interpretation, especially since the associated plate deflection was very small. Consider the static pressure difference near the entrance where it was reported to have the maximum deflection. If one assumes this pressure difference over the entire plate, according to one test, the maximum displacement would be 5% of the channel width. With the same assumptions, all of the other single plate

tests would have much less deflection. Calling this small deflection a collapse velocity does not seem appropriate. Also, it appears that the plate entrance edges were sharp and, if this was the case, it would account for some of the very large scatter and inconsistencies in the data.

Groninger and Kane<sup>12</sup> investigated the response of five Zircaloy flat plates with six channels subjected to flow. Tests were done with elevated temperature and room temperature fluids. There isn't enough data to evaluate properly the high temperature test; thus, the room temperature tests are the only ones commented on. The fuel plates began to oscillate (flutter) and touch at a velocity of 1.9 times Miller's collapse velocity. The deflection was a direct function of the flow velocity. A longitudinal standing wave was evident at velocities below the flutter condition. The flutter instability is not the same as a collapse velocity as predicted with the Miller model. When combs were added to the plates, the deflections were much less, and the flutter disappeared. Two characteristics of these tests are that deflections are directly related to the flow velocity and that flutter occurs at the high flow velocities.

Smissaert<sup>13</sup> published results of tests run on flat plate assemblies. The data supported the work by Groninger and Kane.<sup>12</sup> There was no collapse velocity found in flow velocities up to three times the Miller calculated collapse velocity. The plate deflection was directly related to the pressure differential across a plate, which was related to the flow velocity. At a flow velocity of approximately twice the Miller calculated collapse velocity, flutter began to be evident.

Gwaltney and Luttrell<sup>14</sup> extended Miller's collapse theory to involute plates. Sartory<sup>15</sup> developed an analytical model similar to the Miller model for the flow problem as related to the ANS involute plates. The model included flow in two directions, involute plate equations, inlet/outlet conditions, and a representation of the flow friction.

Reutler<sup>16</sup> translated an unpublished manuscript on the stability behavior of the Institut Laue-Langevin (ILL) fuel elements. When tests were run at nominal coolant velocity (15.5 m/s) without combs, considerable problems were evident. The plates pulled away from their support slots, and some flow channels were essentially closed. This result was a surprise, since the design was very similar to HFIR, which has operated without plate problems for years. It appears, in looking at the photographs of the failed plates, that the problems were related to attachments of the plates in the support slots and not to a collapse problem. No plates buckled, i.e., the center of curvature always stayed on the same side of

the plate. The damage was attributed by the investigators to removal of the combs before running the tests, which altered the entrance conditions.

Swinson and Yahr<sup>17</sup> proposed using the dynamic pressure for calculating the upper bound of plate deflection for this flow problem. The dynamic pressure appears to be a conservative upper bound. Experiments using epoxy involute plates and experiments using flat plates all confirm the dynamic pressure to be an upper bound. It is a conservative upper bound in that the tests on the flat plates and the tests on the involute plates all confirm that the actual pressure difference as measured across the plates is on the order of half the dynamic pressure. If an analytical model is developed based on parallel flow that does not require equal mass flow in the channels, some of the trends seen in the data can be predicted. It would be a mistake to assume that such an elementary description as parallel flow can explain this highly turbulent flow problem. However, trends, such as stable flow and an upper bound on the pressure difference across a plate being the dynamic pressure, can be extracted from this flow model. Data taken in the ANS flow loop tend to support this approach.



#### 4. EXPERIMENTAL ARRANGEMENT

The proposed ANS core is composed of two annular assemblies of involute plates as shown in Fig. 2. The upper element has an inside radius of 175 mm and the lower element has an inside radius of 102 mm. The individual plates are involute in shape and use aluminum cladding with a uranium silicide/aluminum mixture core. Figure 3 shows the general plate arrangement in the element. The plates are 1.27-mm thick, and the flow channels are 1.27-mm thick. This report includes data on the second test of the upper (outer) plates and the lower (inner) plates.

As reported in the first test,<sup>1</sup> the plates were modeled full scale using epoxy material. Model theory was used to find the expected response of the prototype to flow. The model laws used are developed in the report cited earlier. Forming and preparation of the epoxy plates are also discussed in the earlier report. Five active plates and six flow channels were used in the test. The closed flow test loop is illustrated in Fig. 4. Flow entered at the bottom of the test model and was straightened in a single involute channel. Figure 5 pictures the flow straightener for the lower element. The flow straightener's involute cross-sectional dimensions for the upper plates were 13.97-mm wide by 70.3-mm arc length. For the lower plates' flow straightener, the dimensions were 13.97-mm wide by 87.35-mm arc length. The longitudinal length of both flow straighteners was 527 mm. The flow, on leaving the straightener, passed through the section of the test model containing the plates and then was directed into an exit chamber. Figure 6 shows the test section for the lower element. Because of the boundary conditions involved, the three central plates best modeled the plate response expected in the ANS reactor as a function of coolant flow. Five strain gages were located on each of the three central plates. The gages were located, with respect to the plate length, at the entrance, the quarter point, the half point, the three-quarter point, and the exit. The four flow channels bounding the three central plates each contained five static pressure taps located in the same cross-sectional plane as the strain gages. The static pressure taps were located in the outer fixed boundary and were 1.27 mm outside diameter and 1.07 mm inside diameter. Prior to the assembly of the test section, the gages were calibrated to signal the maximum plate deflection of the five cross sections noted because of a pressure difference across the plate. Figure 7 shows a plate being set up for calibration. The longitudinal boundaries were clamped to the aluminum involute mandrel. The maximum plate deflection was monitored with a dial

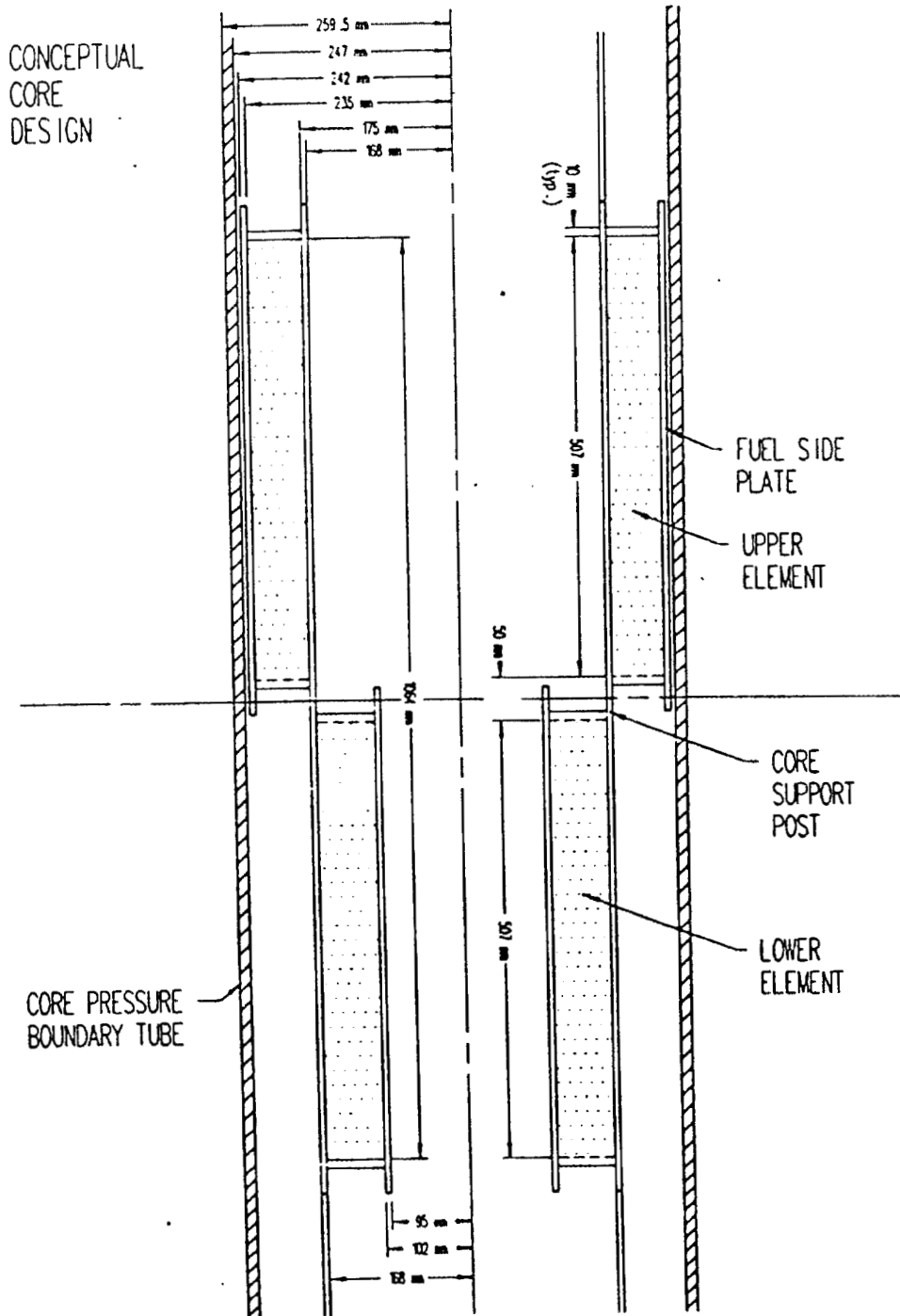


Fig. 2. Conceptual core design.

indicator. The strain signals were recorded as a function of the pressure load applied to the plate. The pressure was vacuum applied by first sealing the plate ends with a pliable clay and pumping through the pressure tubes shown in Fig. 7. It was evident that the readings from the strain gages at the entrance and exit of the plate were affected by the pliable clay during calibration. Therefore, for calibration, the average readings from the other gages versus deflection were used.

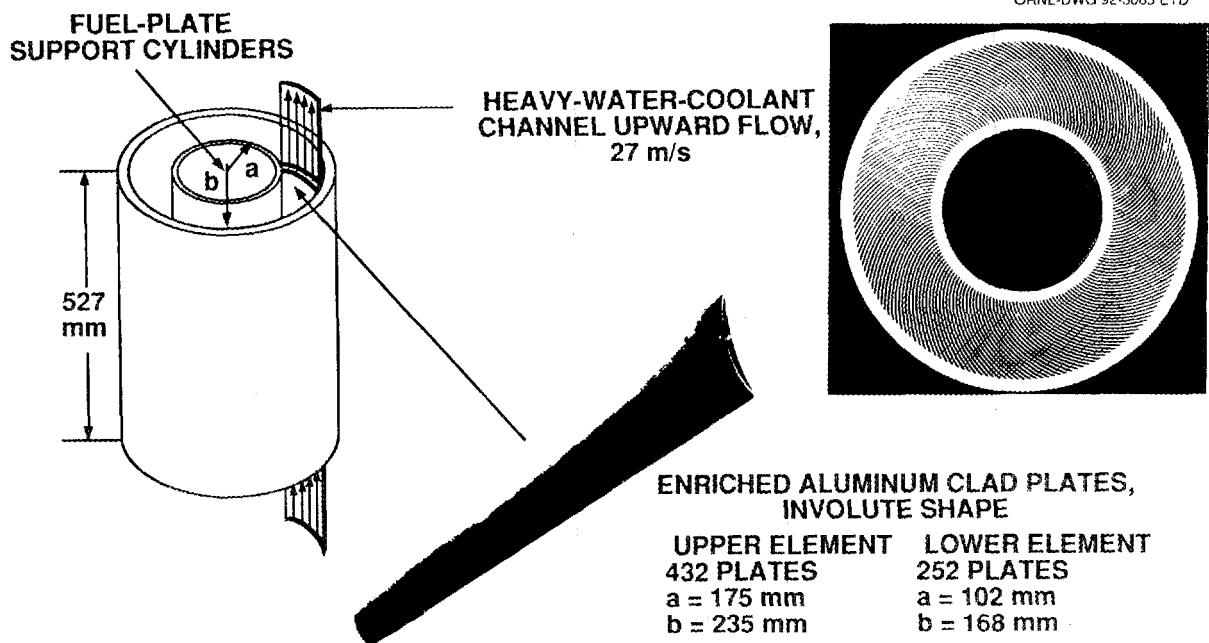


Fig. 3. Plate arrangement in support cylinders.

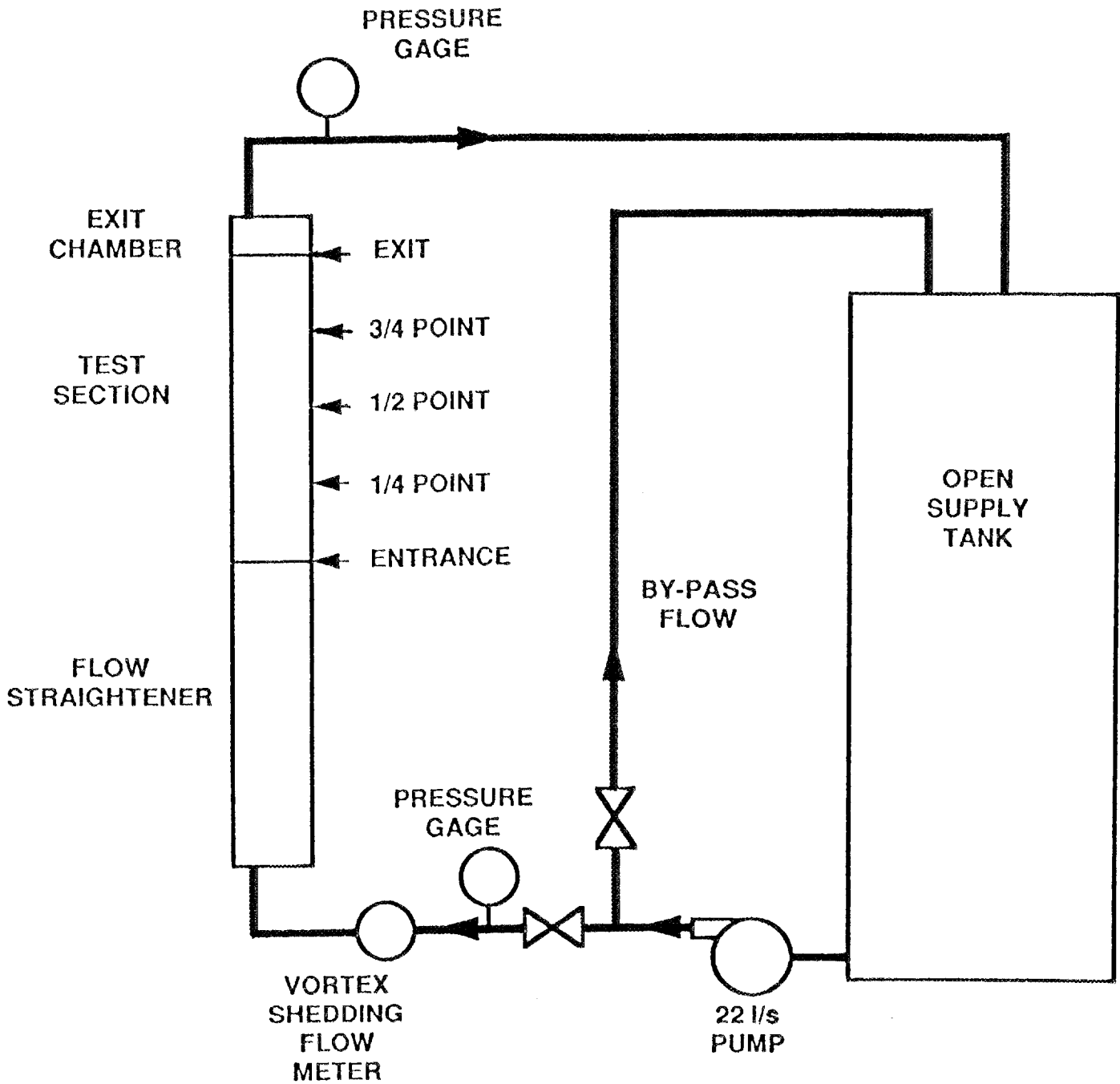
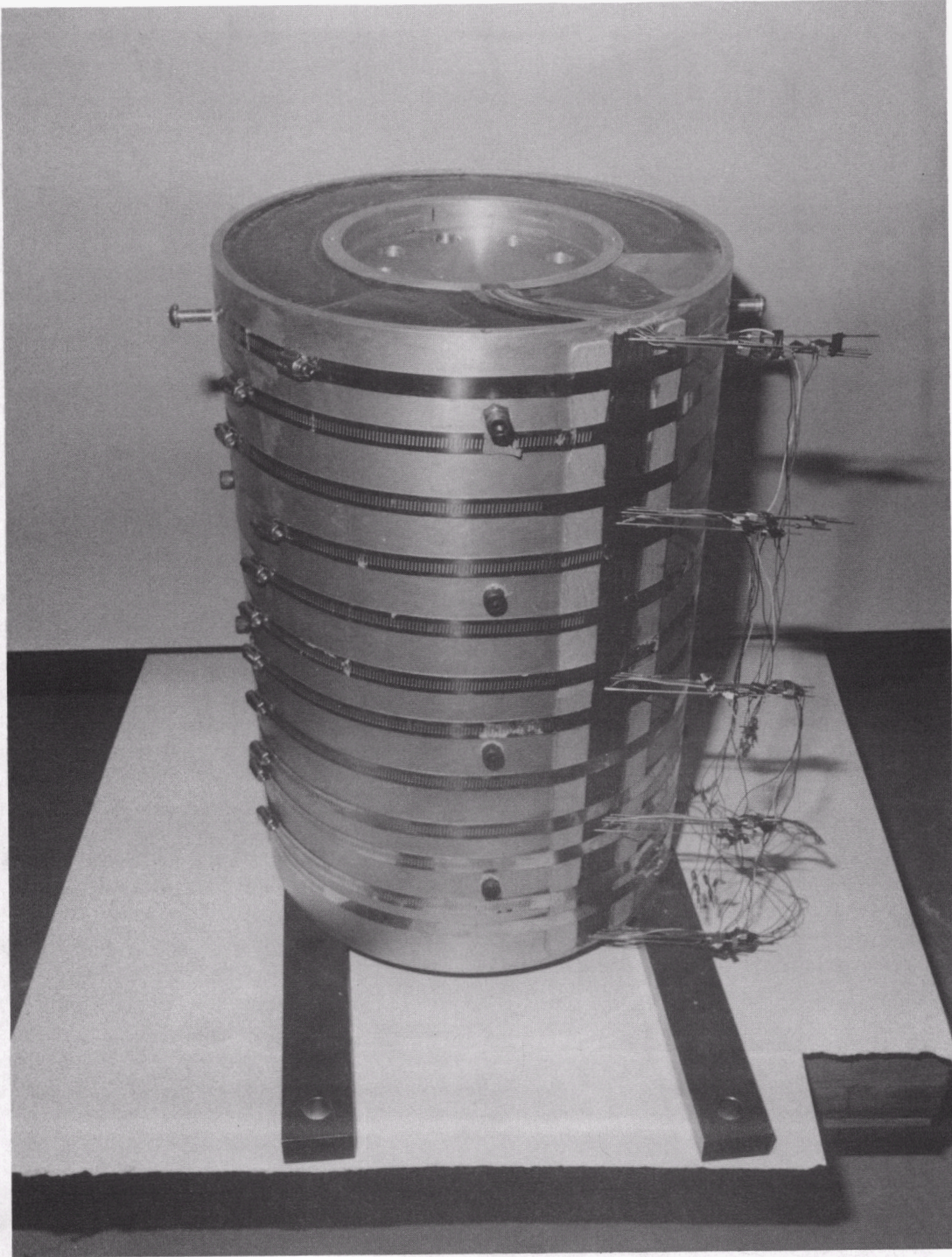


Fig. 4. Flow test loop.



**Fig. 5. Flow straightener for the lower element.**



**Fig. 6. Lower plate test element.**

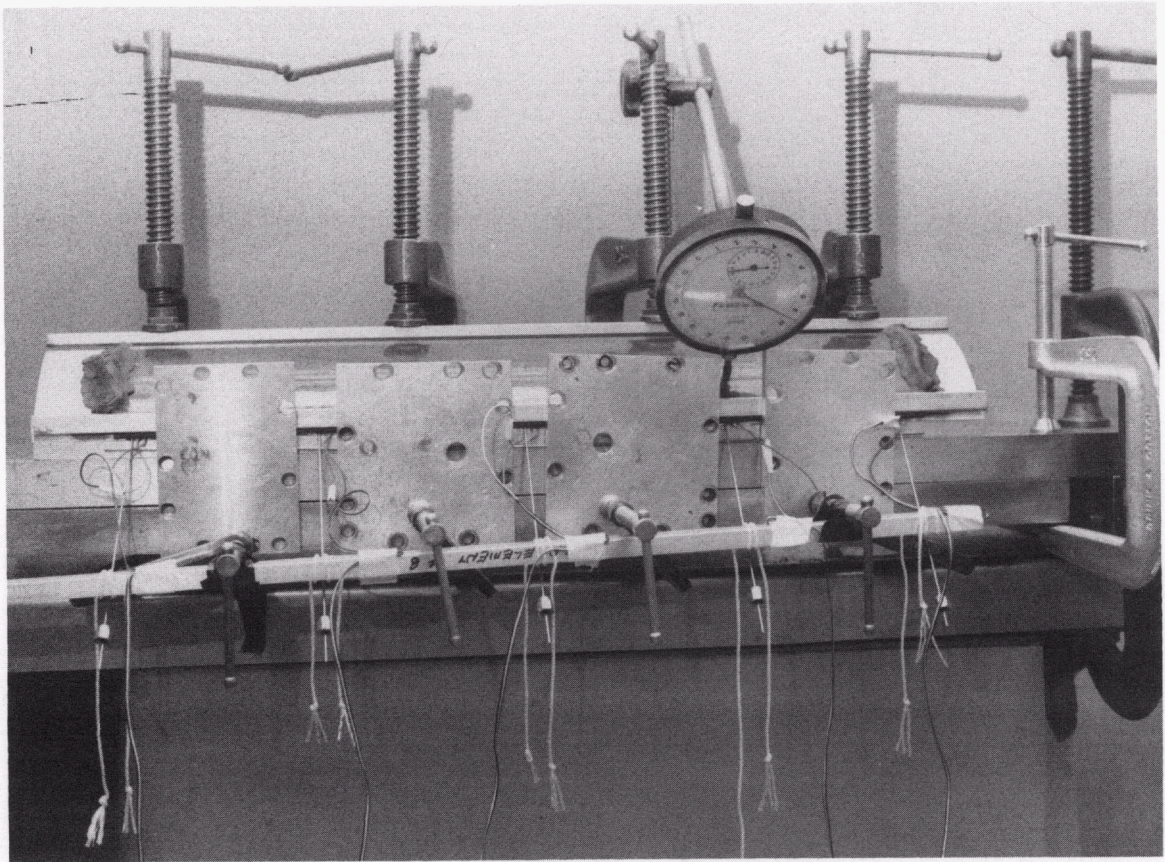


**Fig. 7. Plate calibration arrangement.**



## 5. DATA AND RESULTS FROM SECOND TEST OF THE ANS PLATES

As the plates were fabricated, a number was assigned to each plate. Some of the plates were not in a thickness tolerance band of  $\pm 0.05$  mm and were not used in the test elements. No particular numbering scheme was used in stacking the plates for assembly. The plates in the upper test section are identified: the central plate is labeled A8; the first plate on the concave side of the central plate is A1; the second plate on the concave side of the central plate is A5; the first plate on the convex side of the central plate is A4; and the second plate on the convex side of the central plate is A9. The average modulus of elasticity for the strain-gaged plates A8, A1, and A4 was experimentally found to be  $3183 \text{ MPa} \pm 12\%$  ( $461,721$  psi). The experimental arrangement to find the modulus was the same optical technique as reported in ORNL/TM-12353.<sup>1</sup>

The plates in the lower test section are identified: the central plate is labeled B4; the first plate on the concave side of the central plate is B14; the second plate on the concave side of the central plate is B6; the first plate on the convex side of the central plate is B15; and the second plate on the convex side of the central plate is B18. The average modulus of elasticity for the strain-gaged plates B4, B14, and B15 was found to be  $3563 \text{ MPa} \pm 3.5\%$  ( $516,827$  psi).

As in the earlier tests, the data collected was computer controlled and included the flow volume from a vortex shedding meter, the 15 strain gages, the upstream and downstream pressures, pressure from each of the 20 pressure taps in the flow channels, and the water temperature. The entrance strain gage for the central plate was monitored with a strip chart recorder to detect plate response as a function of time and flow. Generally, data were recorded with the computer taking three sets of zero data (i.e., without flow), which took about 30 s; next, the flow was adjusted to the desired value, and three sets of loaded data were recorded; and lastly, flow was stopped, and three more zero data sets were recorded. This procedure allowed for inspection of the data to detect any significant variation that might negate a test.

During the process of gathering data for the lower element, one of the plates fractured. In comparison to all of the other plate tests, this was a premature failure in that much higher flow velocities were realized in the other tests before failure occurred. The epoxy material is a brittle material, and it is reasoned that an unknown crack because of fabrication and/or

assembly was present in one of the plates. The result of this was an early failure as the load was increased because of flow. At the beginning of this program, the very first plate that was being calibrated shattered at a very low pressure load. It seemed evident at that time that precautions were needed to help avoid cracks and to prevent premature plate failure. It appears, however, that a crack still went undetected and caused an early plate failure during the second test of the lower plates. The data that were collected is reported.

The pressure drop along the length of a channel is illustrated in Figs. 8–17. The channel identification number references the plates that bound the channel. The pressure drop was found by subtracting the pressure reading at the exit to the channel from the pressure reading at the entrance to the channel.

The maximum deflections of the three instrumented upper plates and the three instrumented lower plates as a function of prototype flow velocity are shown in Figs. 18–27. For comparative purposes, the coordinate positions of the three instrumented plates for the upper and lower models at the entrance, the quarter, the half, the three-quarter, and the exit cross sections are shown in the graphs. The central plate is positioned at the zero coordinate. The plate on the concave side of the central plate is positioned at +1.27 mm. The plate on the convex side of the central plate is positioned at -1.27 mm. As the plates are loaded by the flow, the coordinates of the plates change.

Figures 28–33 show the deflection pattern of each of the gaged plates at different flow velocities.

Pressure data were taken at the entrance, the quarter point, the half point, the three-quarter point, and the exit point in each of the four channels that surrounded the gaged plates. For presentation, the pressure difference across each plate was calculated from the pressure readings and scaled to an equivalent deflection reading. The scale factor was taken from the calibration data, where deflection was recorded as a function of pressure difference across a plate. The results are shown in Figs. 34–43. Some comments are made in the next section about the function relating the plate deflection to the flow velocity being similar to the function relating the dynamic pressure to the flow velocity. Therefore, the dynamic pressure has been scaled using the same constant, experimentally relating the pressure differential to plate deflection and compared in Figs. 44–53 to the plate deflections measured experimentally during flow.

Figures 54 and 55 show selected responses of the plate strain gages as a function of time to illustrate the type of vibration that was sensed by the plates.

This second round of data using new test models was taken to give a larger data base for drawing conclusions. Figures 56-59 show all deflection data at the entrance and at the three-quarter point versus prototype flow velocity for the upper plate test sections and for the lower plate test sections. These two cross sections were the most significant in that the largest deflections were found at these points.

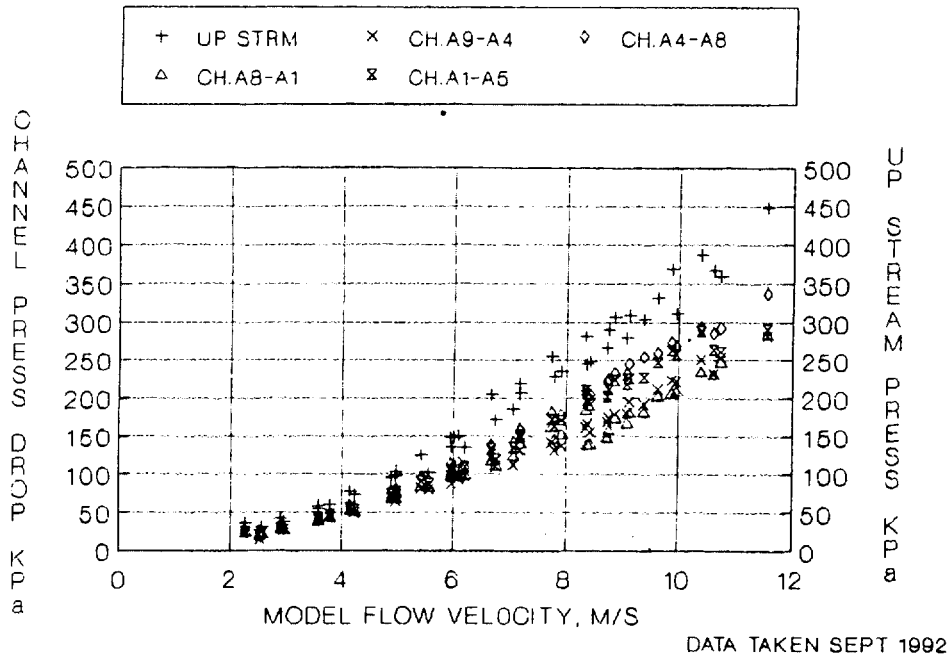


**Fig. 8. Channel pressure drop vs velocity, second model upper ANS plates, all channels.**

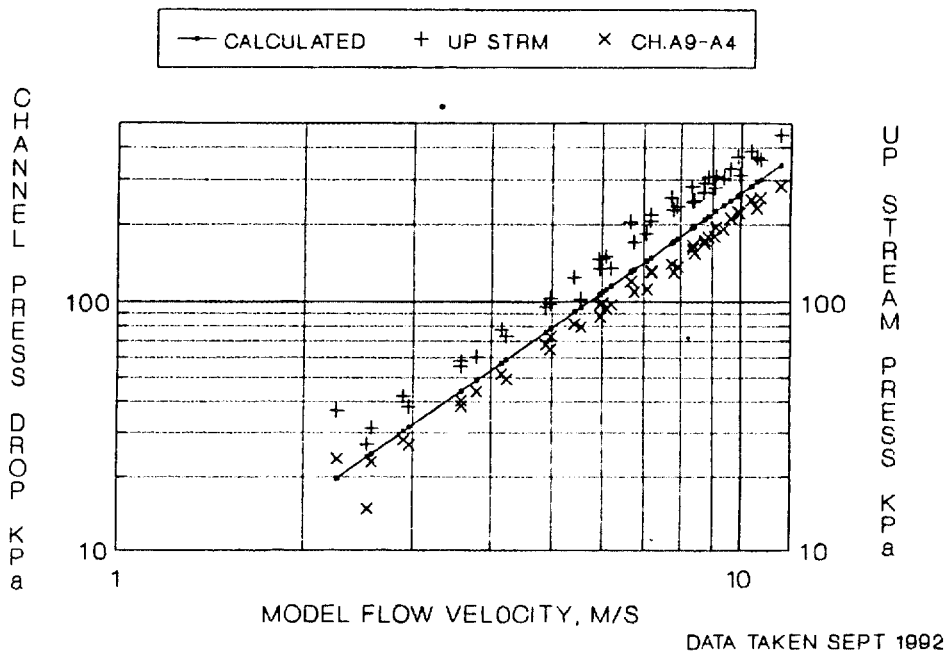


**Fig. 9. Channel pressure drop vs velocity, second model upper ANS plates, Channel A9-A4.**

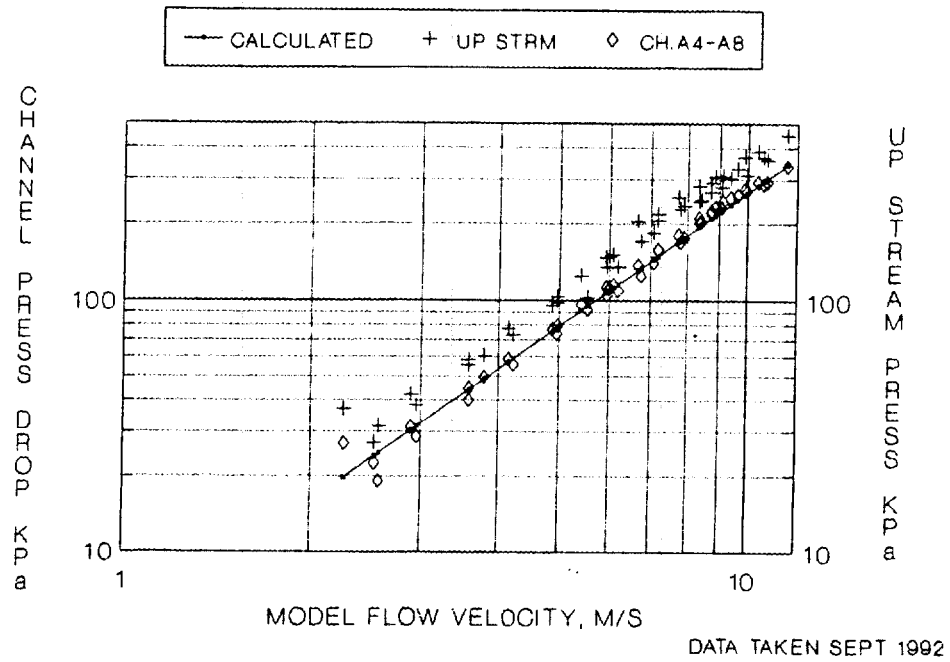


**Fig. 10. Channel pressure drop vs velocity, second model upper ANS plates, Channel A4-A8.**

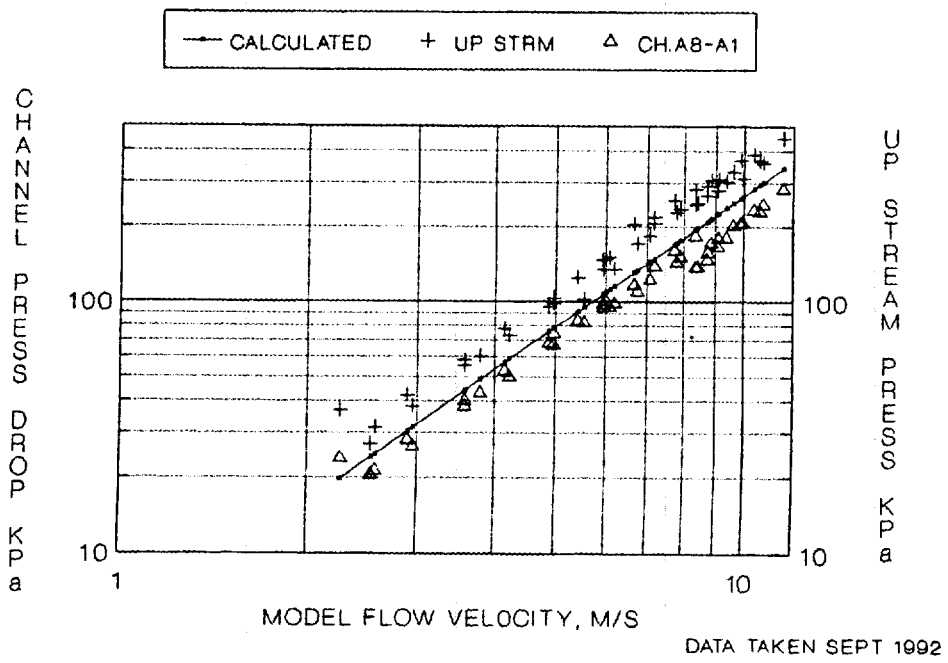


**Fig. 11. Channel pressure drop vs velocity, second model upper ANS plates, Channel A8-A1.**

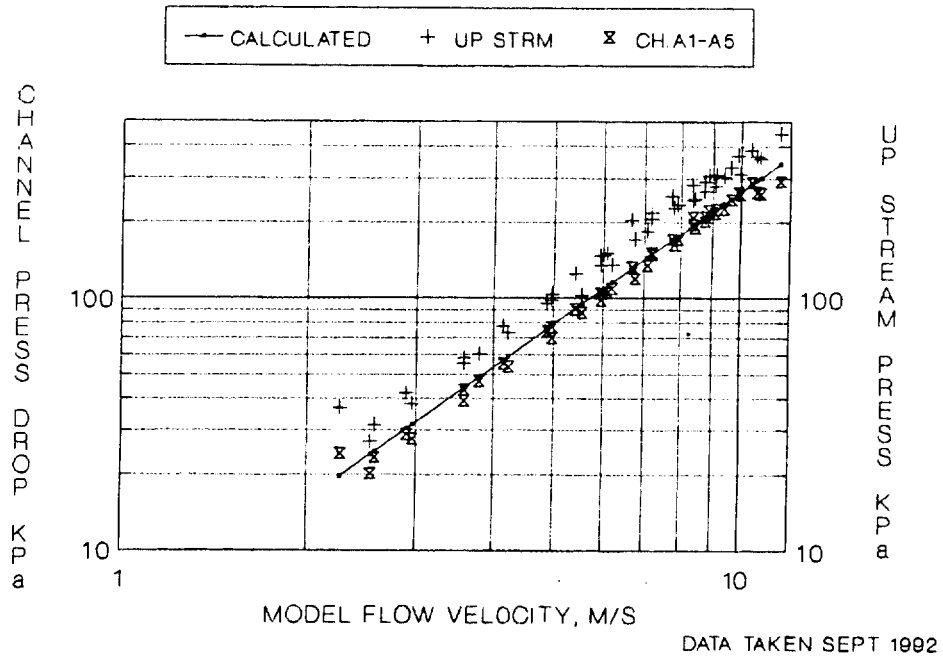


**Fig. 12. Channel pressure drop vs velocity, second model upper ANS plates, Channel A1-A5.**

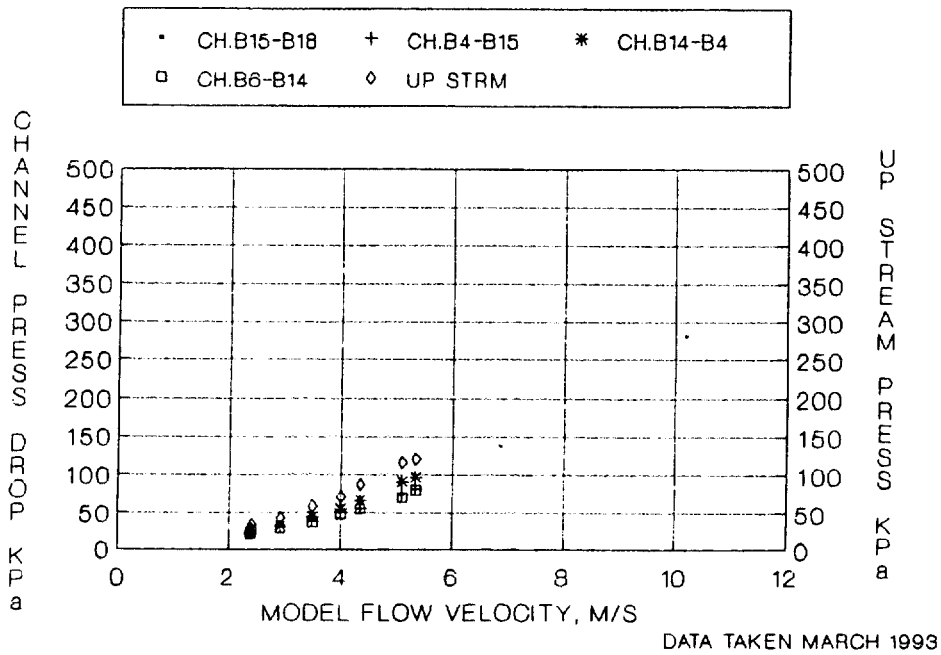


**Fig. 13. Channel pressure drop vs velocity, second model lower ANS plates, all channels.**

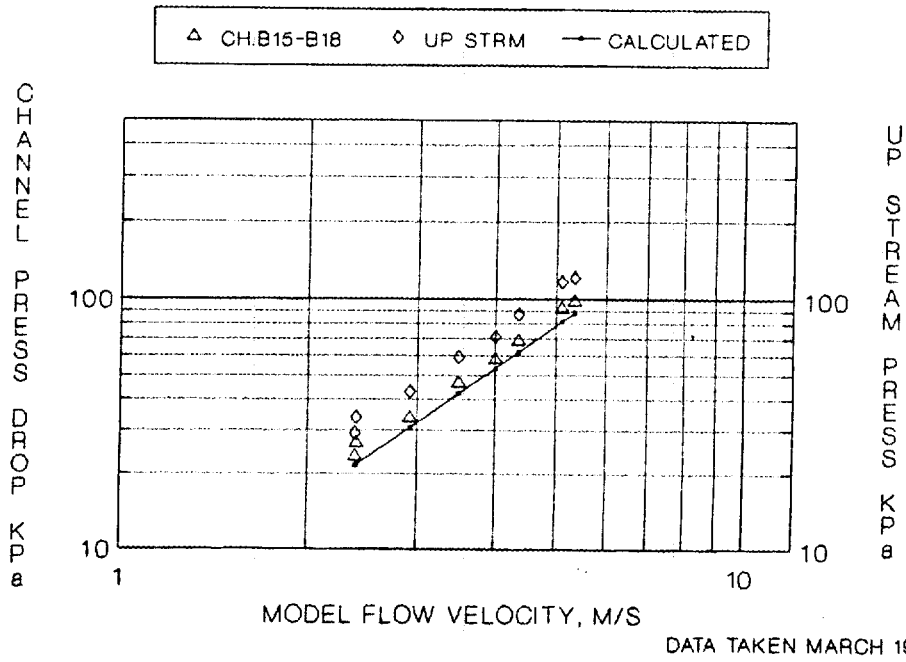


**Fig. 14. Channel pressure drop vs velocity, second model lower ANS plates, Channel B15-B18.**

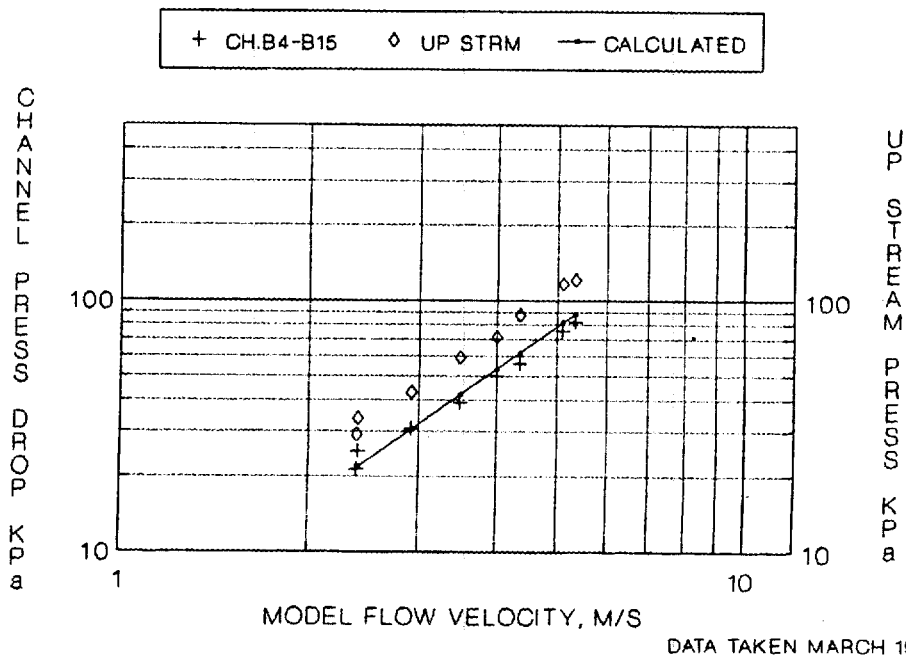


**Fig. 15. Channel pressure drop vs velocity, second model lower ANS plates, Channel B4-B15.**

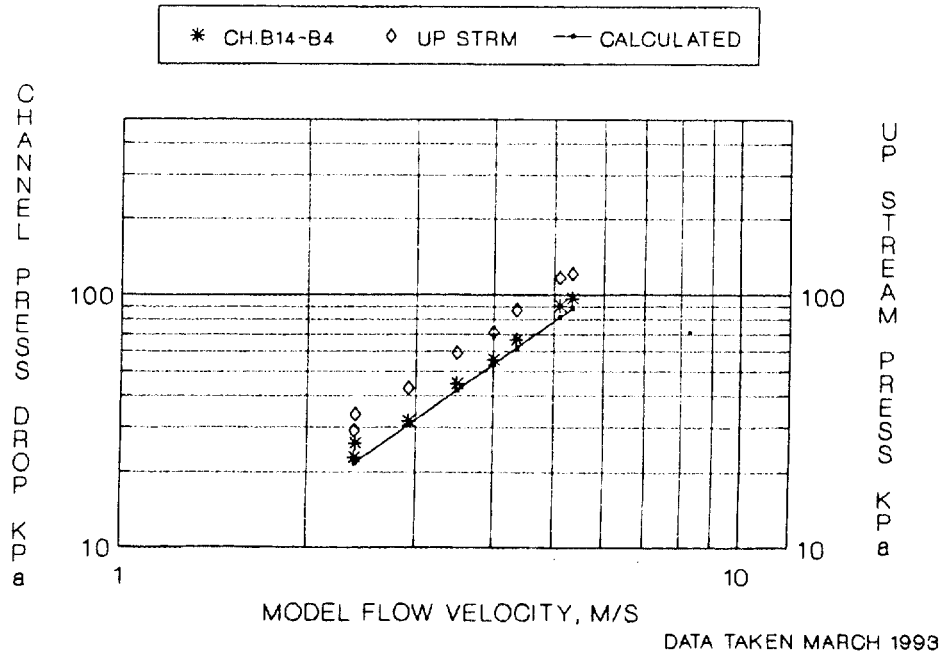


**Fig. 16. Channel pressure drop vs velocity, second model lower ANS plates, Channel B14-B4.**

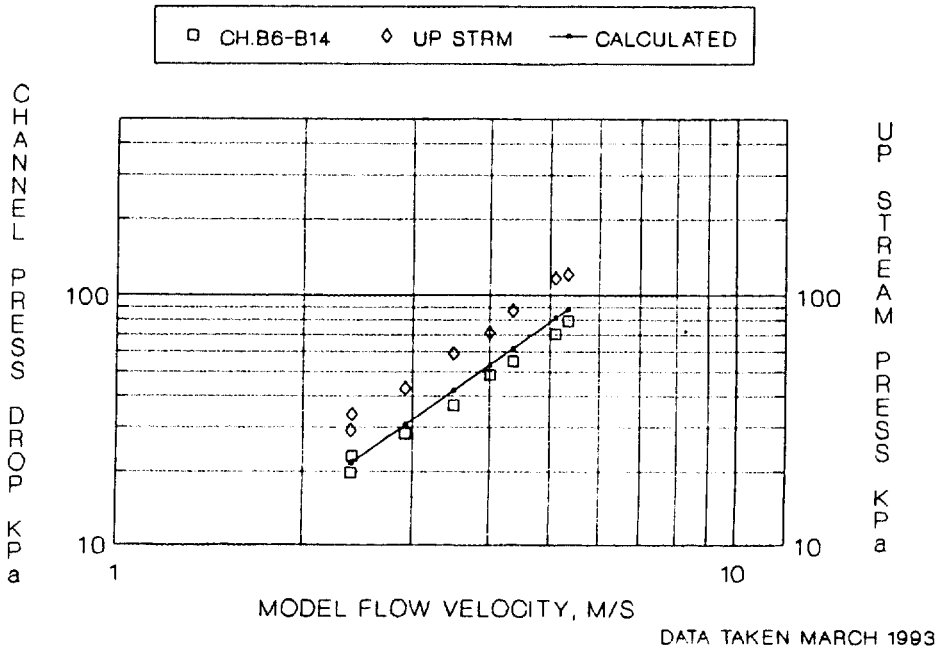


**Fig. 17. Channel pressure drop vs velocity, second model lower ANS plates, Channel B6-B14.**

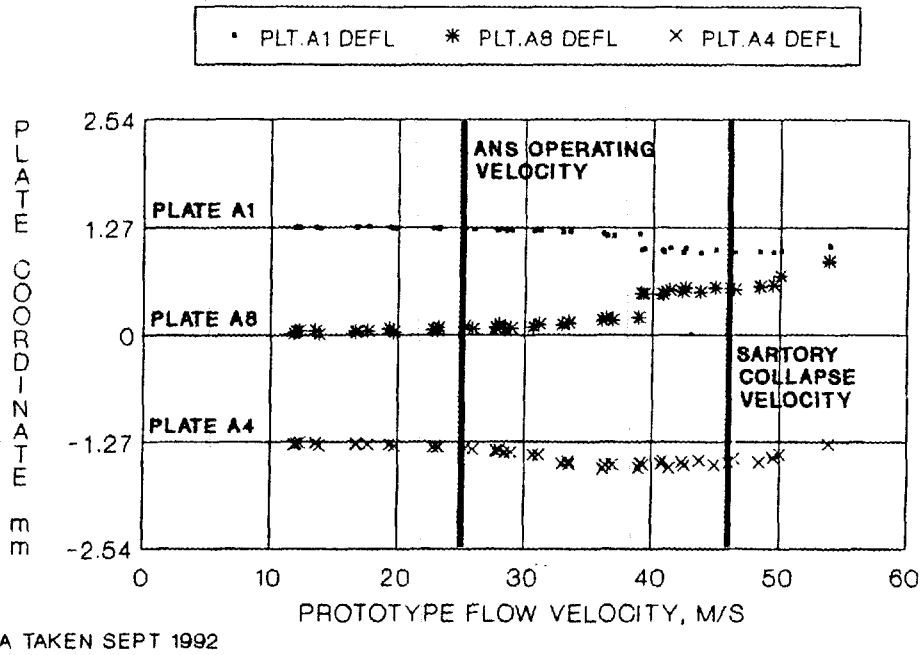


Fig. 18. Plate A1, A8, A4 entrance deflection, second model upper ANS plates.

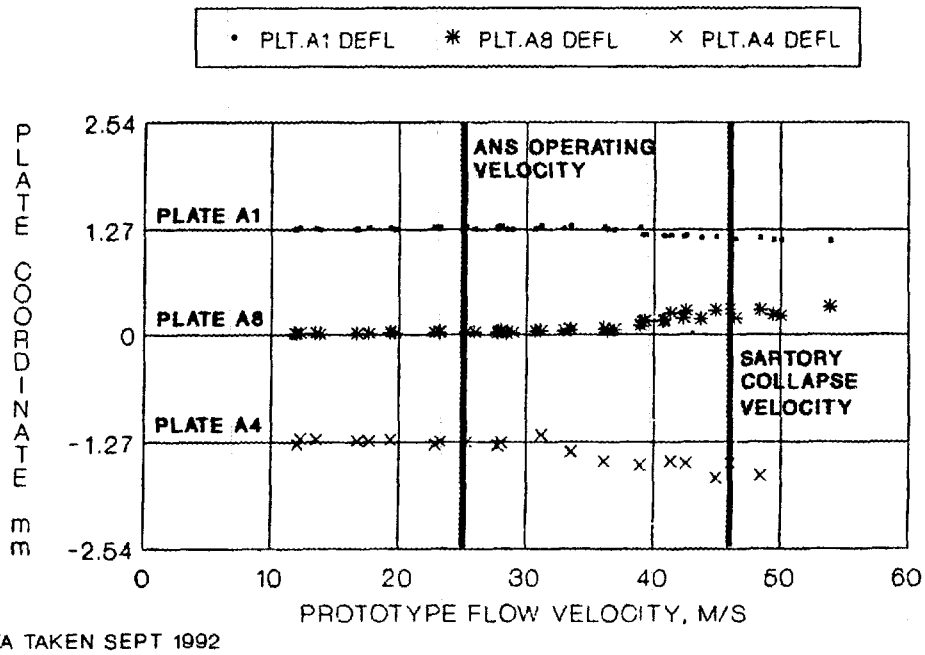


Fig. 19. Plate A1, A8, A4 quarter point deflection, second model upper ANS plates.

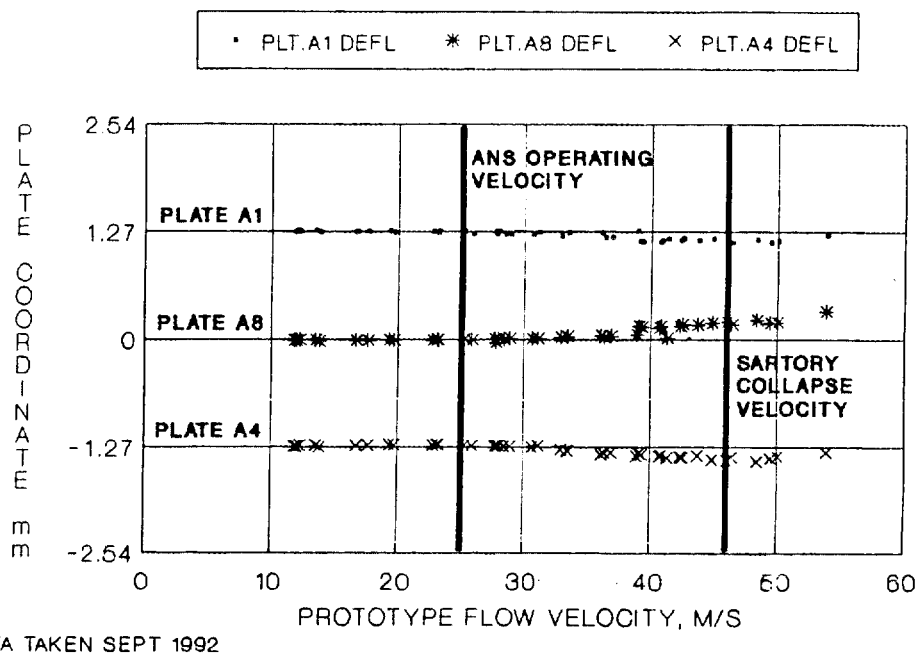


Fig. 20. Plate A1, A8, A4 half point deflection, second model upper ANS plates.

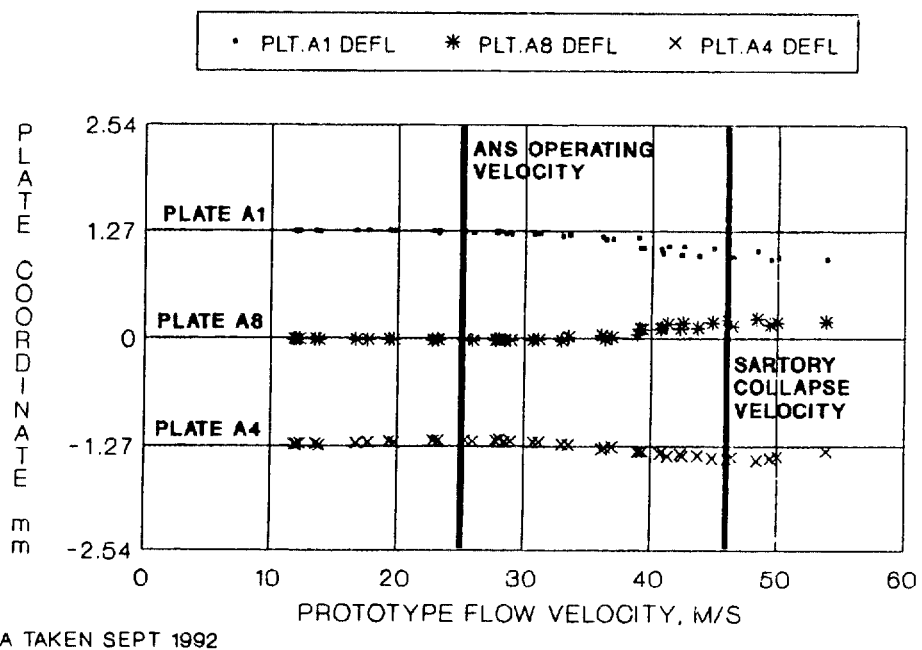


Fig. 21. Plate A1, A8, A4 three-quarter point deflection, second model upper ANS plates.

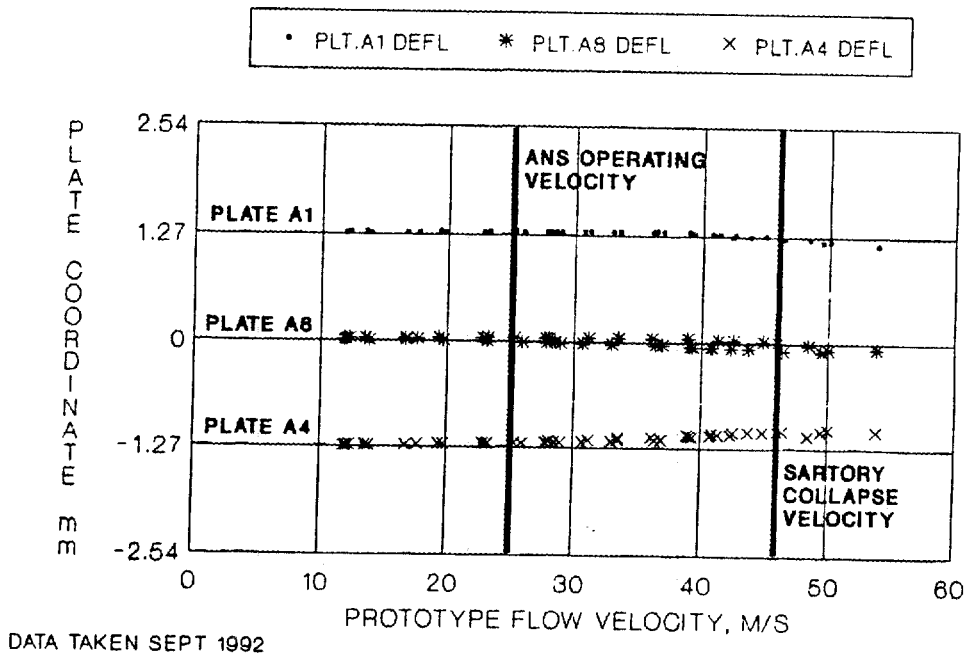


Fig. 22. Plate A1, A8, A4 exit deflection, second model upper ANS plates.

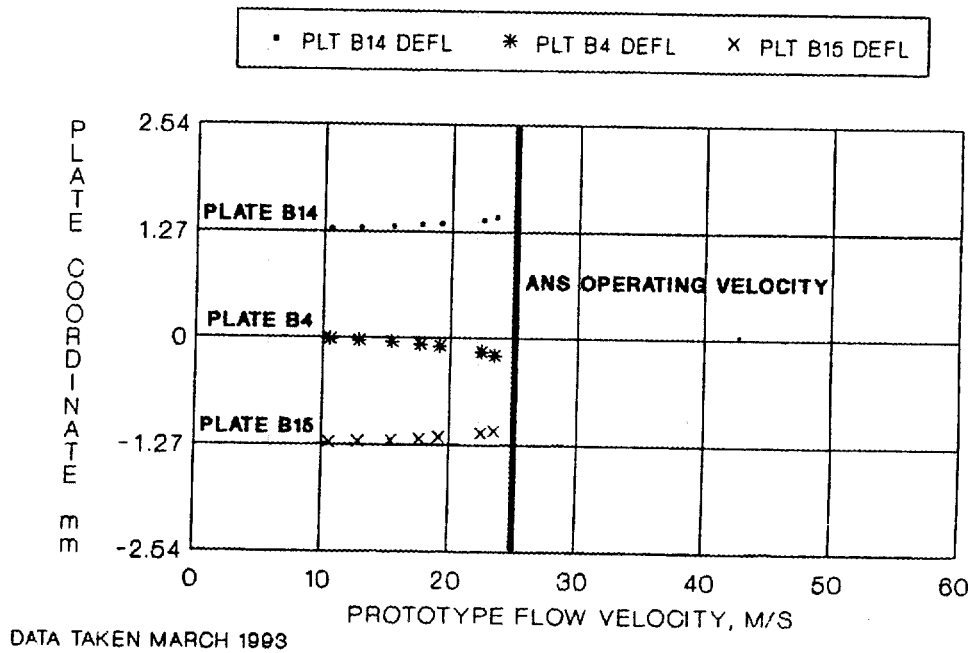
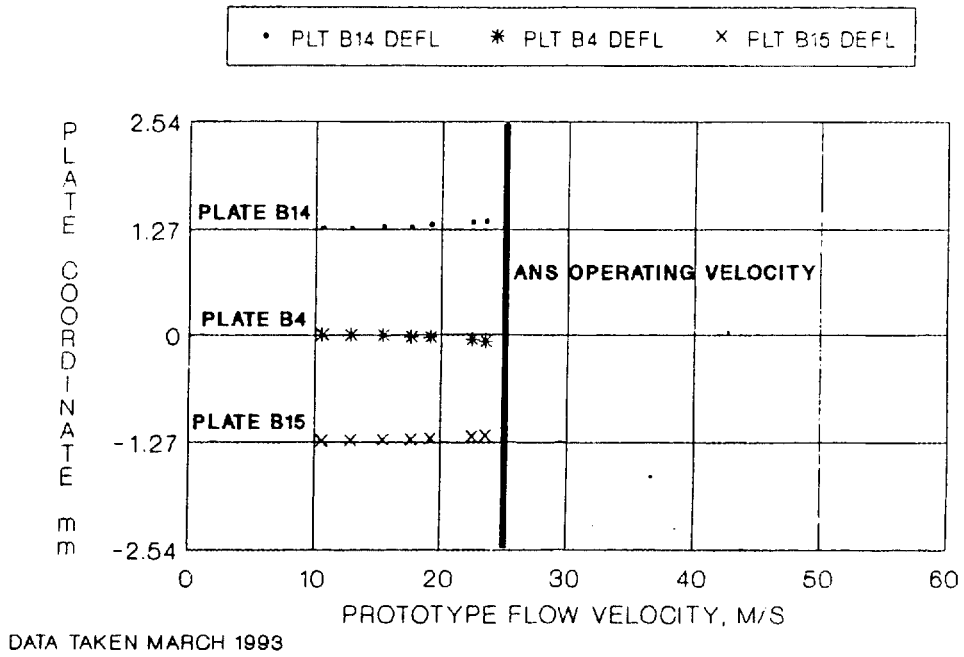
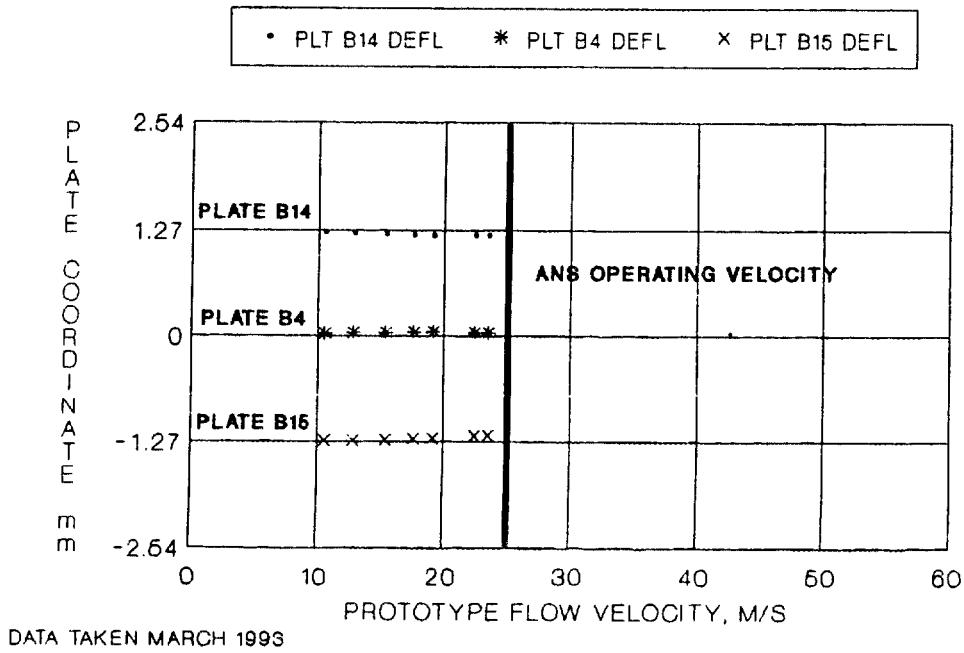


Fig. 23. Plate B14, B4, B15 entrance deflection, second model lower ANS plates.



**Fig. 24. Plate B14, B4, B15 quarter point deflection, second model lower ANS plates.**



**Fig. 25. Plate B14, B4, B15 half point deflection, second model lower ANS plates.**

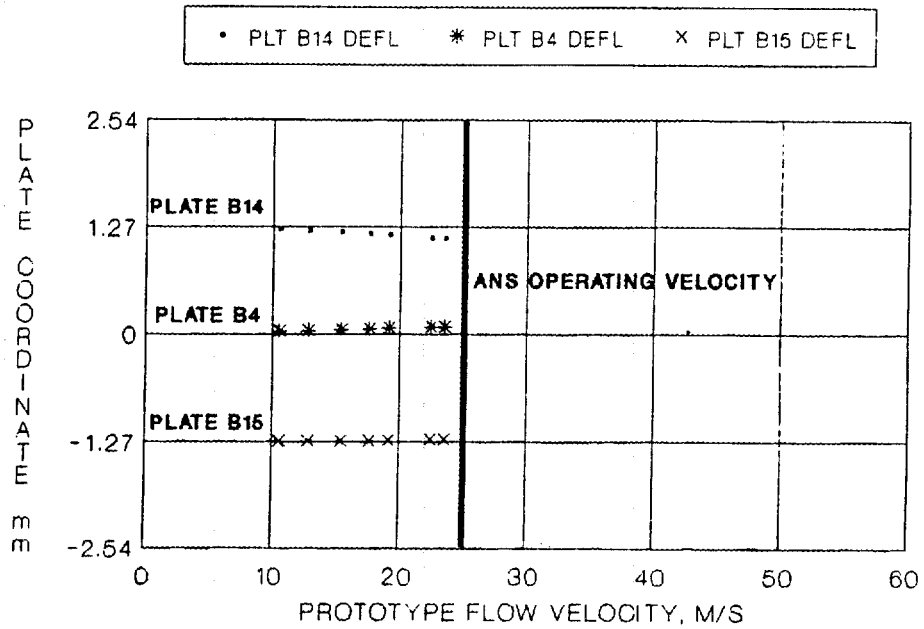


**Fig. 26. Plate B14, B4, B15 three-quarter point deflection, second model lower ANS plates.**

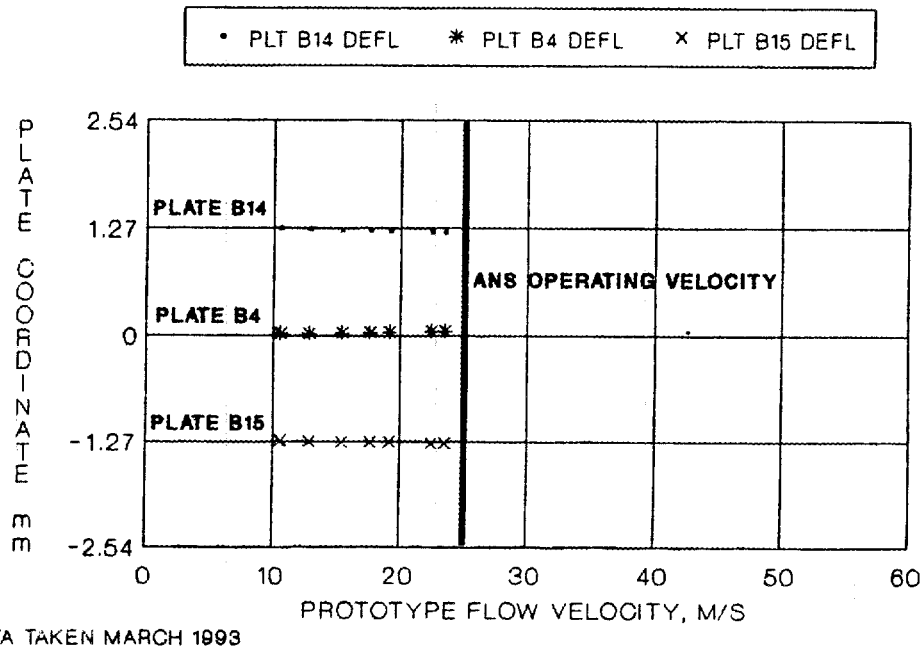


**Fig. 27. Plate B14, B4, B15 exit deflection, second model lower ANS plates.**

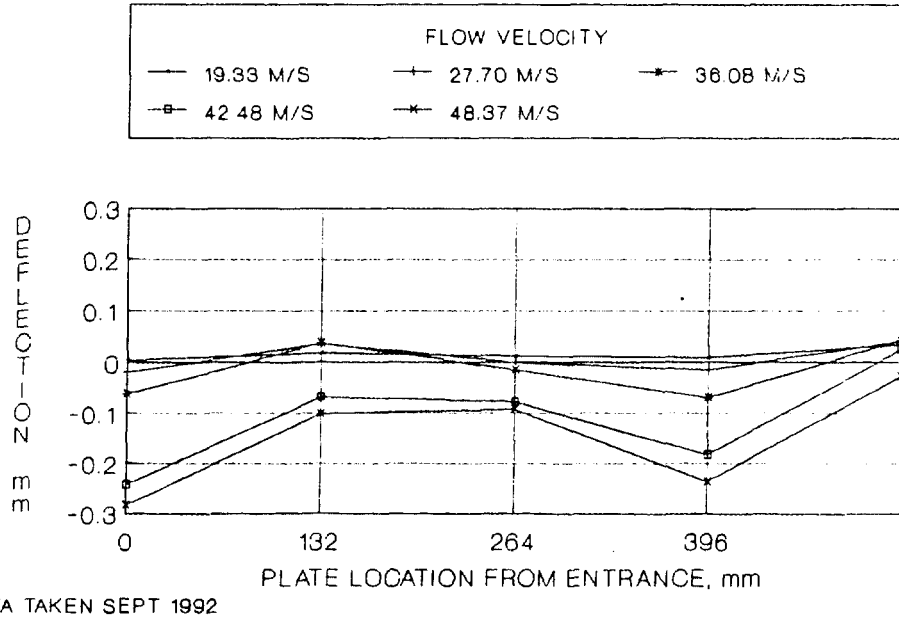


**Fig. 28. Upper element plate A1 vs position on plate at different prototype velocities, second test on upper element.**

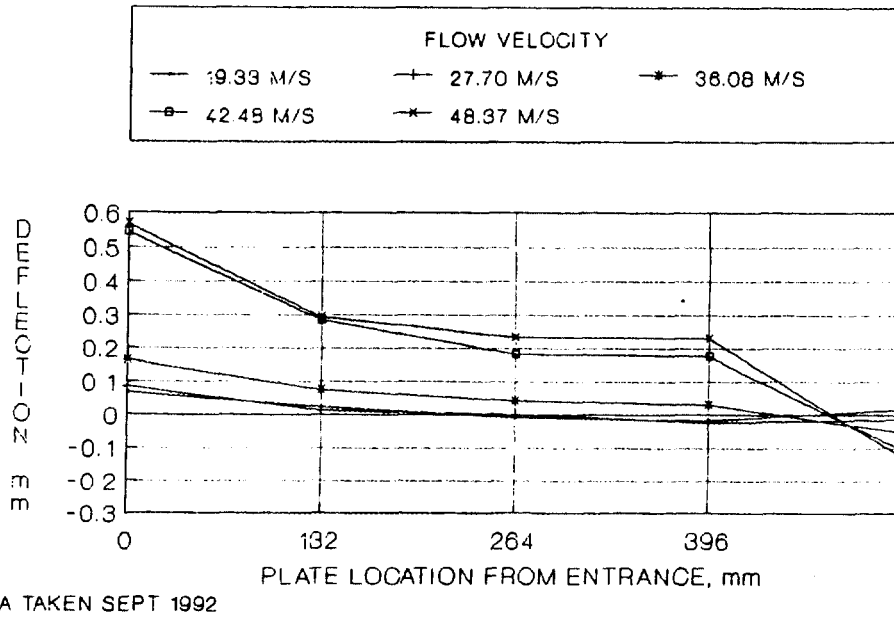
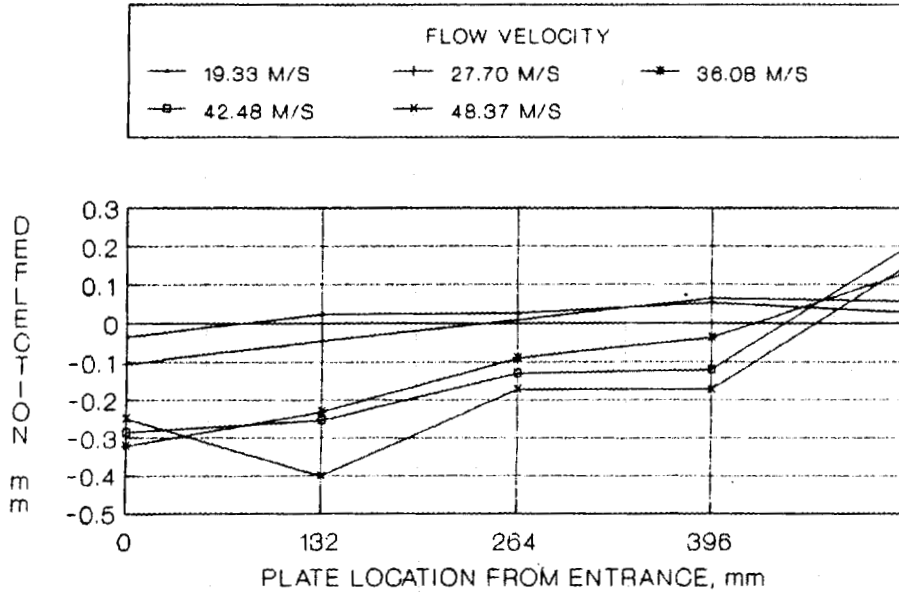
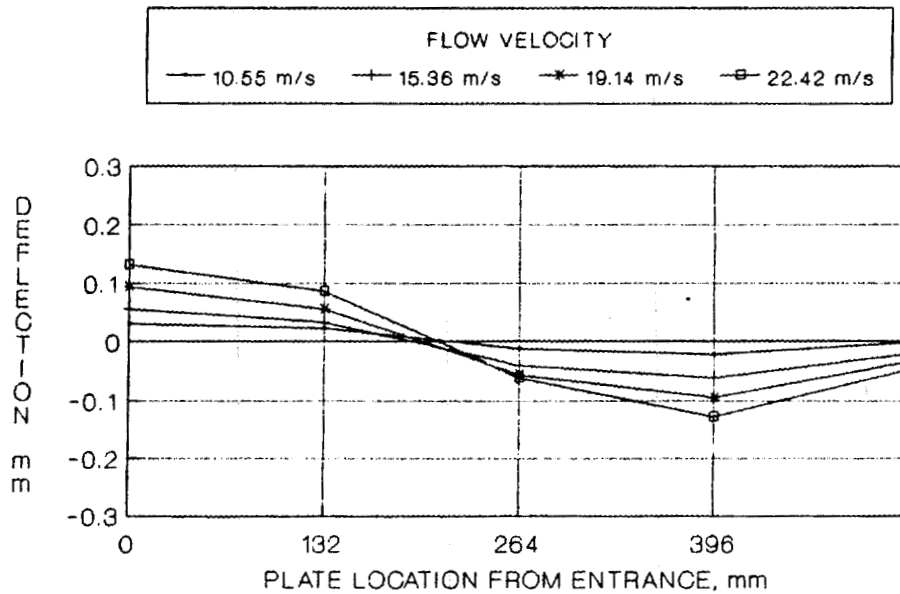


**Fig. 29. Upper element plate A8 vs position on plate at different prototype velocities, second test on upper element.**



DATA TAKEN SEPT 1992

**Fig. 30. Upper element plate A4 vs position on plate at different prototype velocities, second test on upper element.**



DATA TAKEN MARCH 1993

**Fig. 31. Lower element plate B14 vs position on plate at different prototype velocities, second test on lower element.**

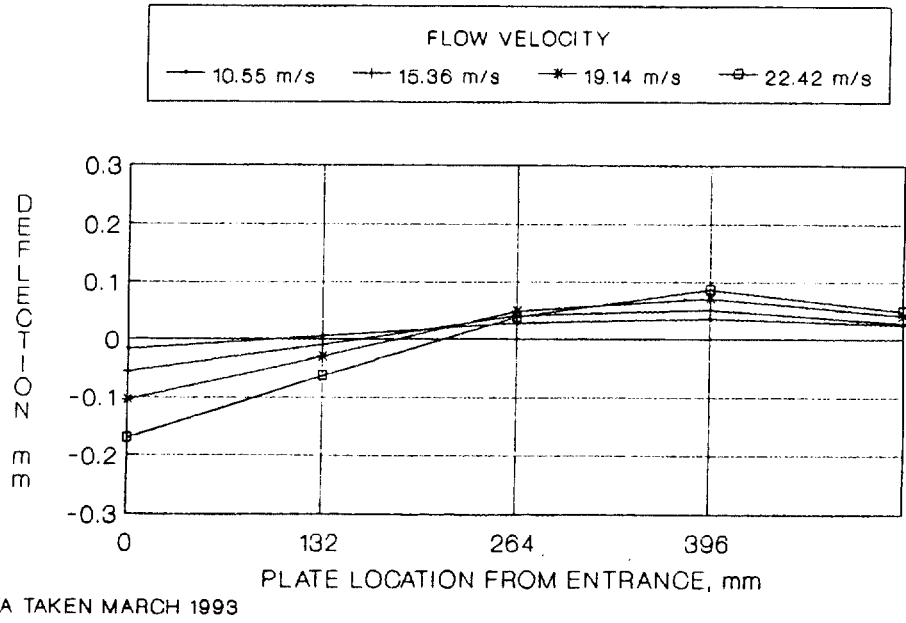


**Fig. 32. Lower element plate B4 vs position on plate at different prototype velocities, second test on lower element.**

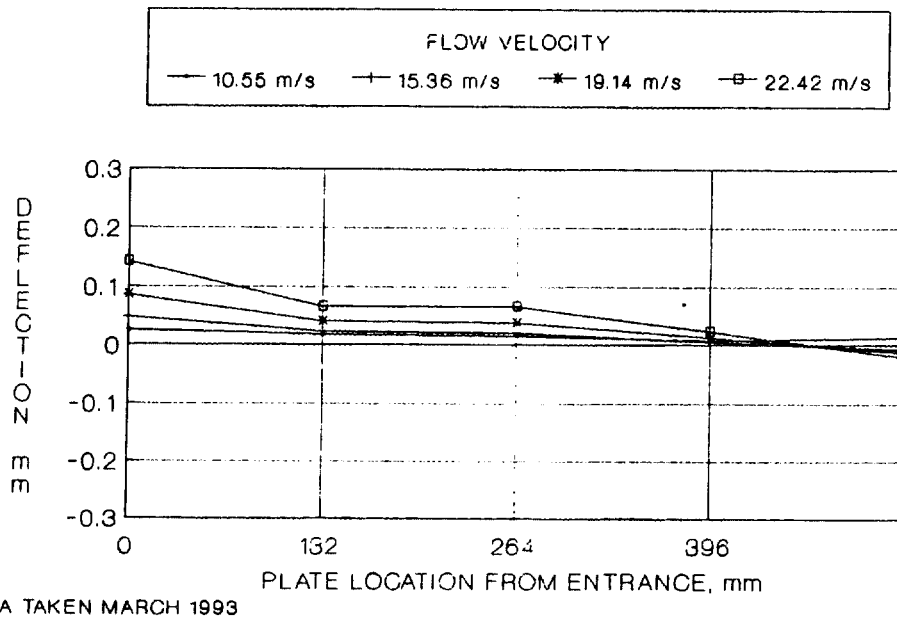


**Fig. 33. Lower element plate B15 vs position on plate at different prototype velocities, second test on lower element.**

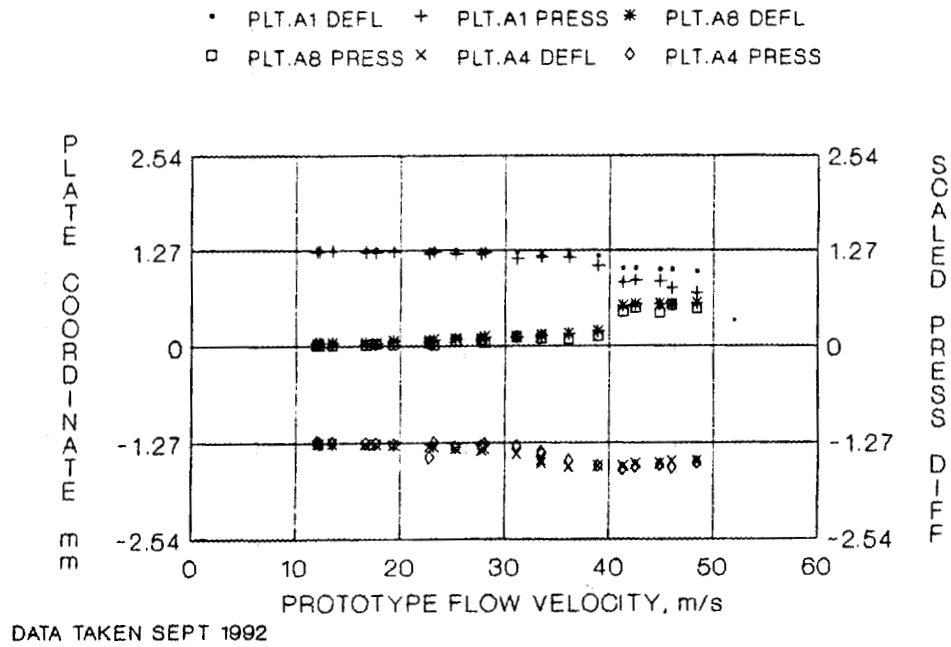


**Fig. 34. Plate A1, A8, A4 entrance pressure differential, second model upper ANS plates.**

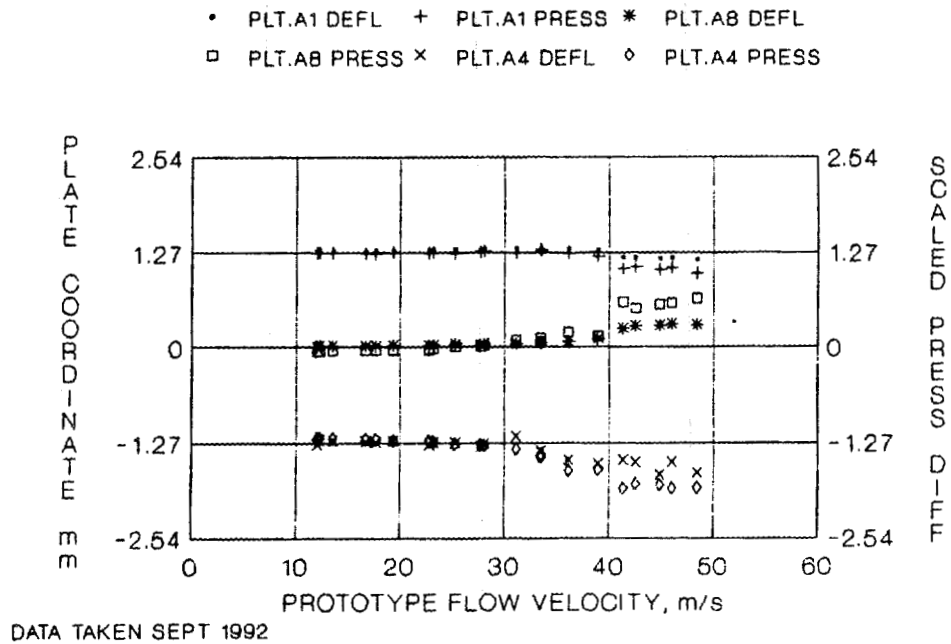


**Fig. 35. Plate A1, A8, A4 quarter point pressure differential, second model upper ANS plates.**

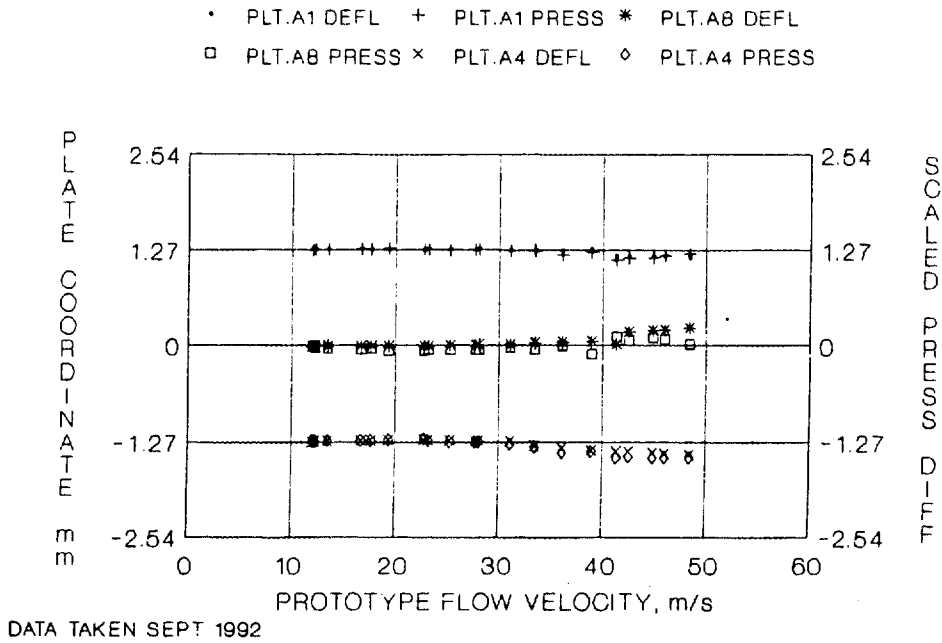


**Fig. 36. Plate A1, A8, A4 half point pressure differential, second model upper ANS plates.**

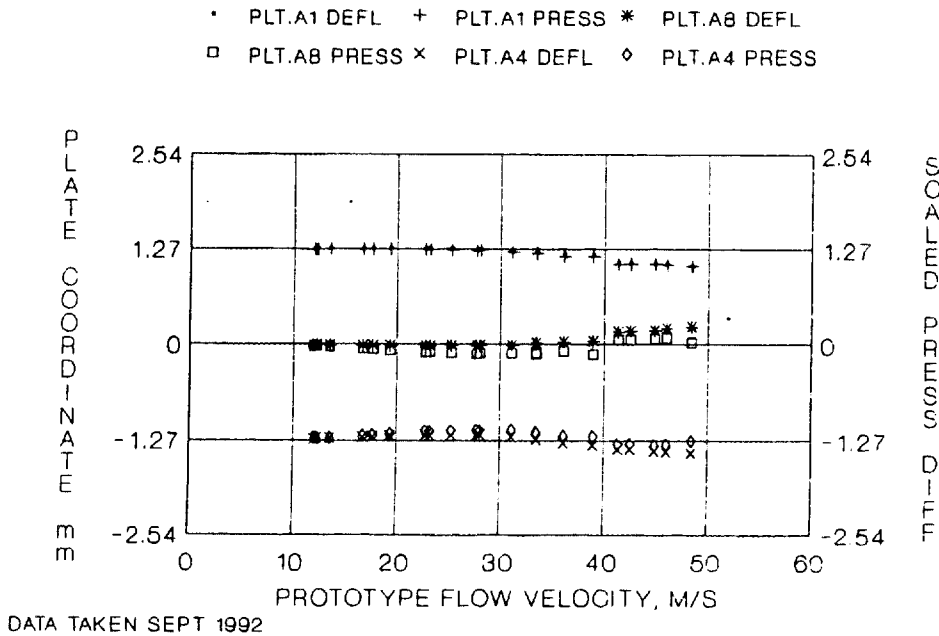


**Fig. 37. Plate A1, A8, A4 three-quarter point pressure differential, second model upper ANS plates.**

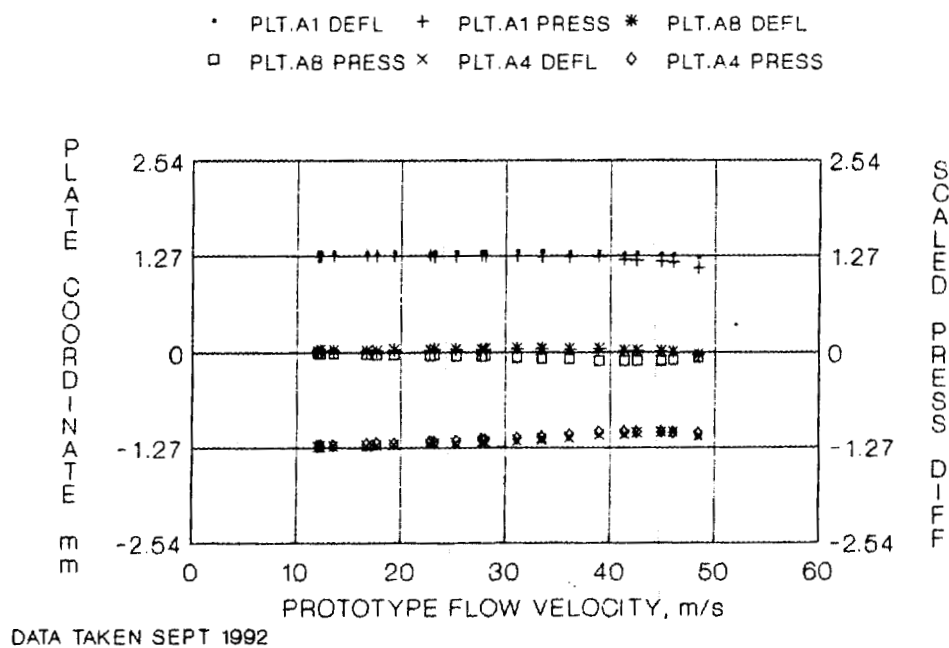


**Fig. 38. Plate A1, A8, A4 exit point pressure differential, second model upper ANS plates.**

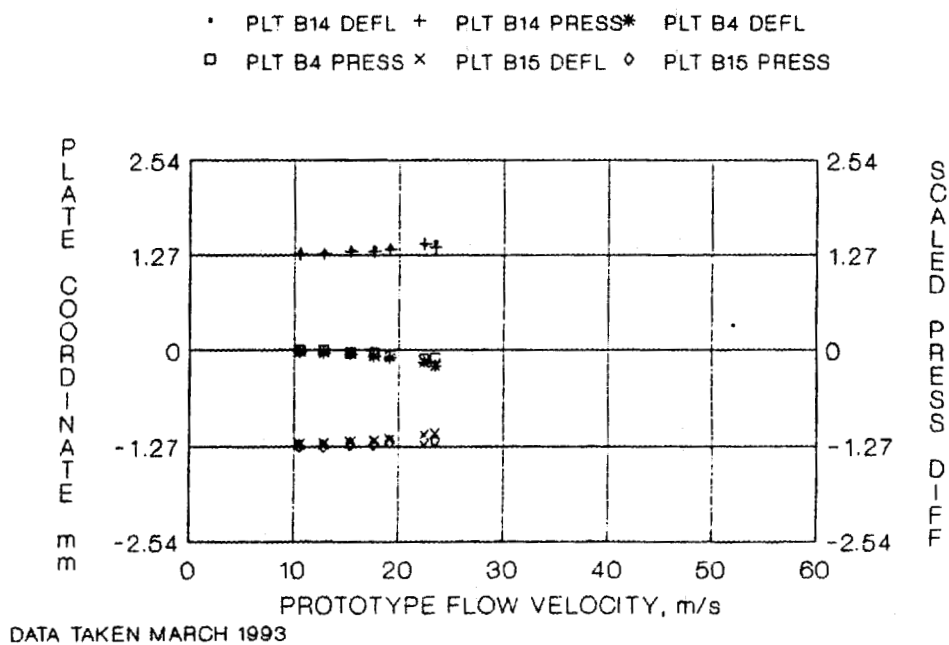


**Fig. 39. Plate B14, B4, B15 entrance pressure differential, second model lower ANS plates.**

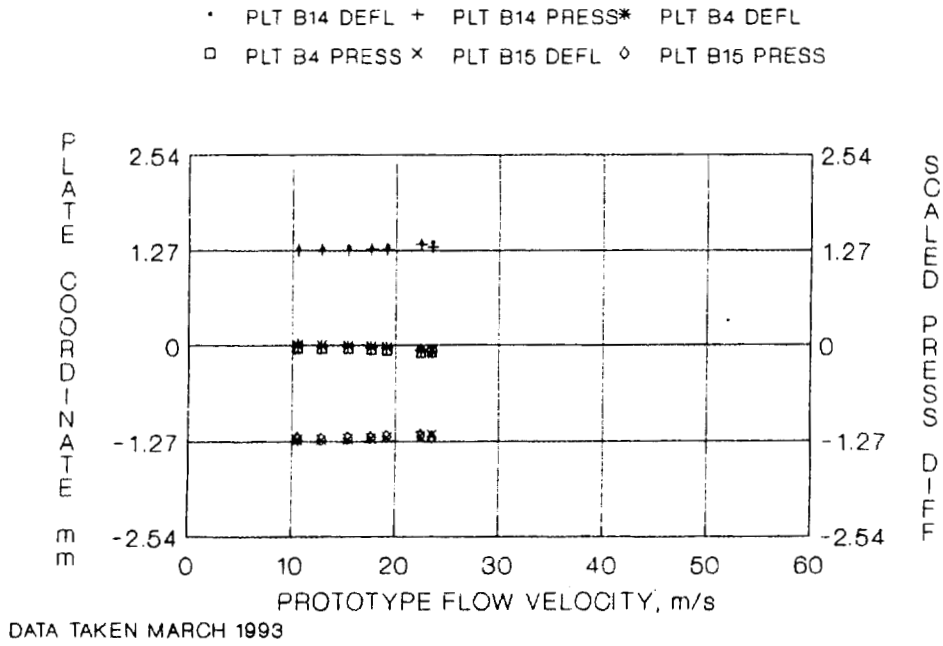


**Fig. 40. Plate B14, B4, B15 quarter point pressure differential, second model lower ANS plates.**

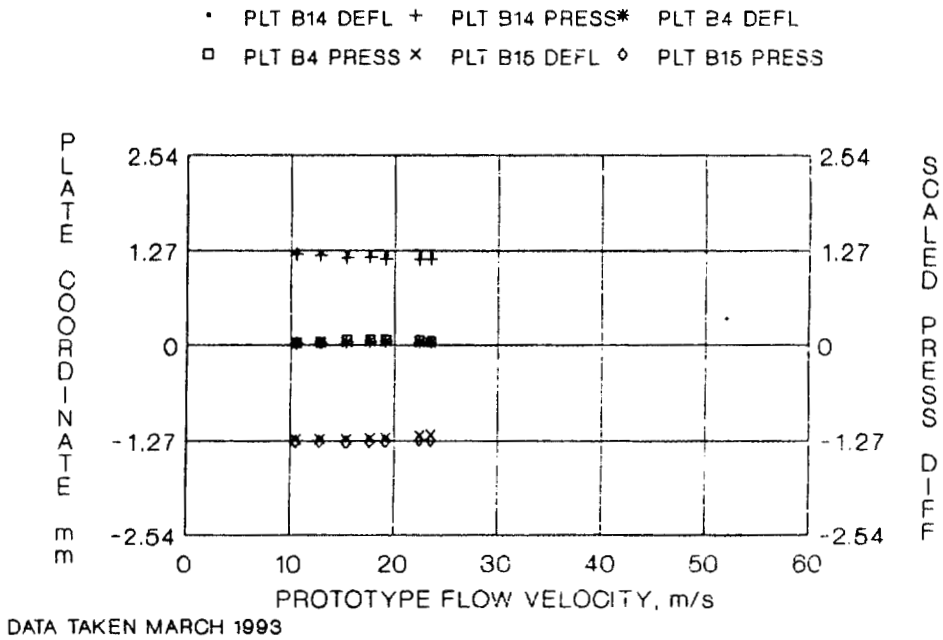


**Fig. 41. Plate B14, B4, B15 half point pressure differential, second model lower ANS plates.**

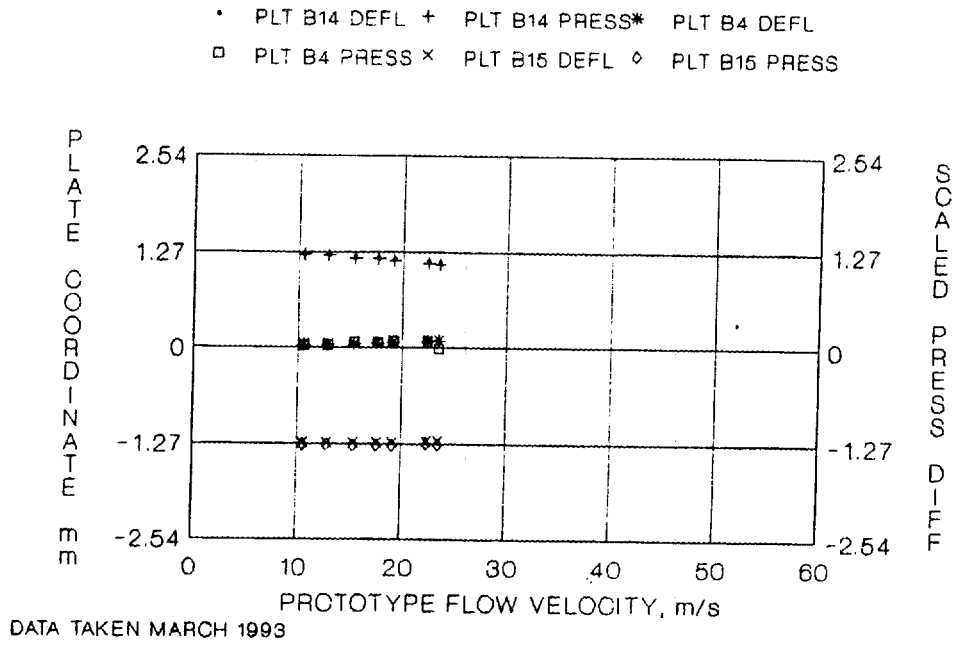


**Fig. 42. Plate B14, B4, B15 three-quarter point pressure differential, second model lower ANS plates.**

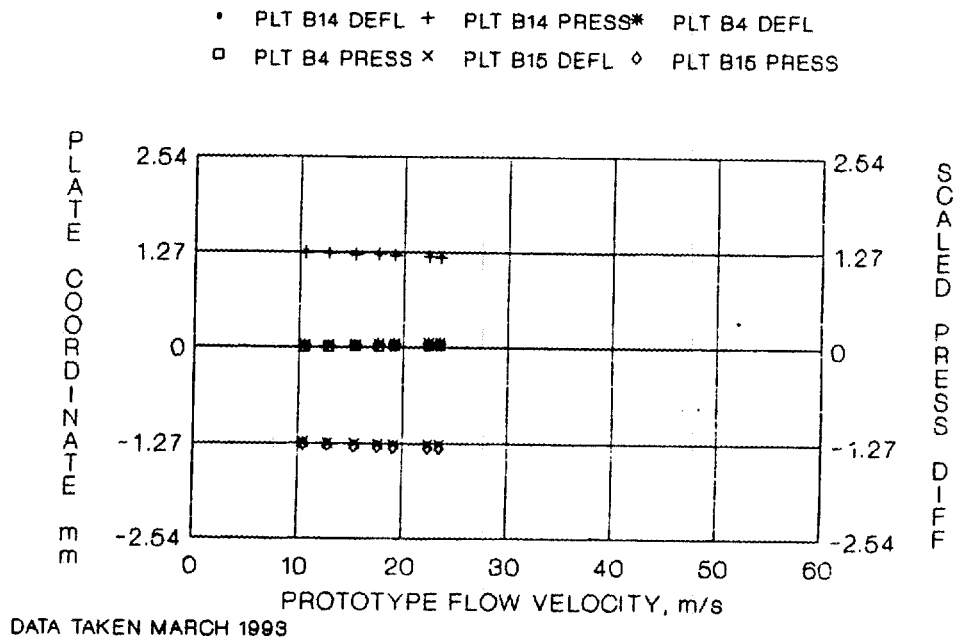


**Fig. 43. Plate B14, B4, B15 exit pressure differential, second model lower ANS plates.**

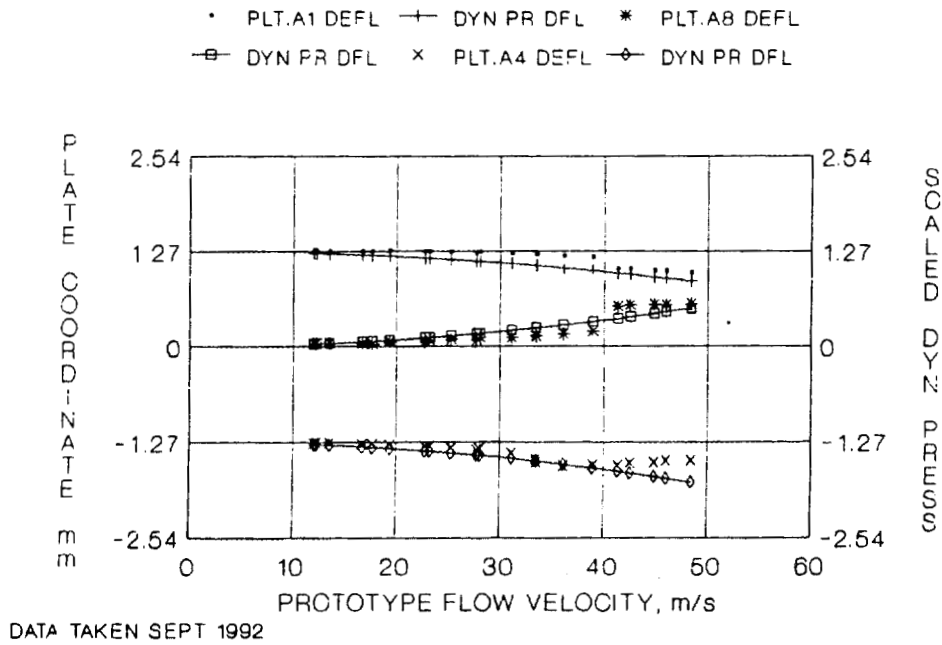


**Fig. 44. Plate A1, A8, A4 entrance dynamic pressure, second model upper ANS plates.**

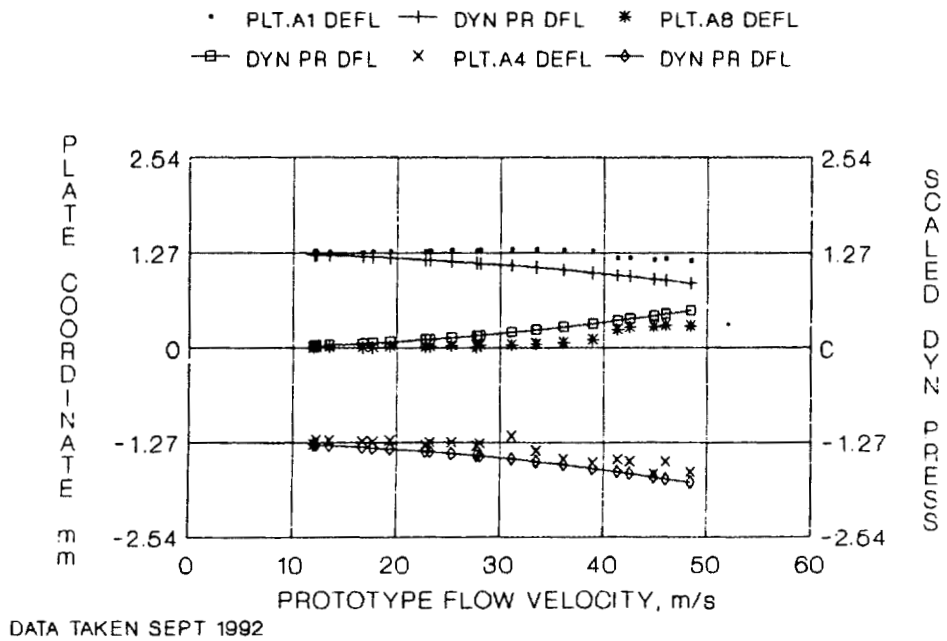


**Fig. 45. Plate A1, A8, A4 quarter point dynamic pressure, second model upper ANS plates.**

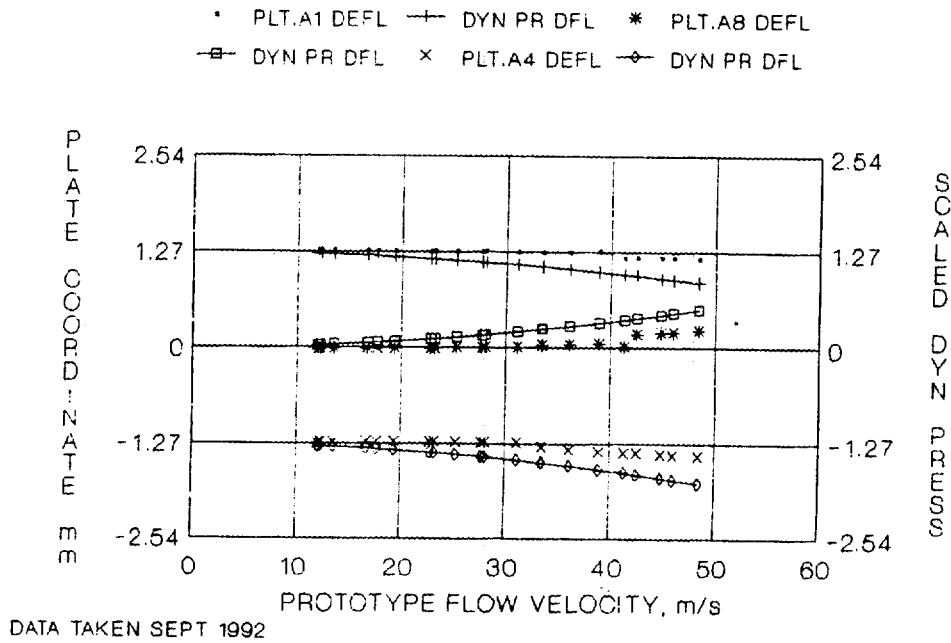


**Fig. 46. Plate A1, A8, A4 half point dynamic pressure, second model upper ANS plates.**

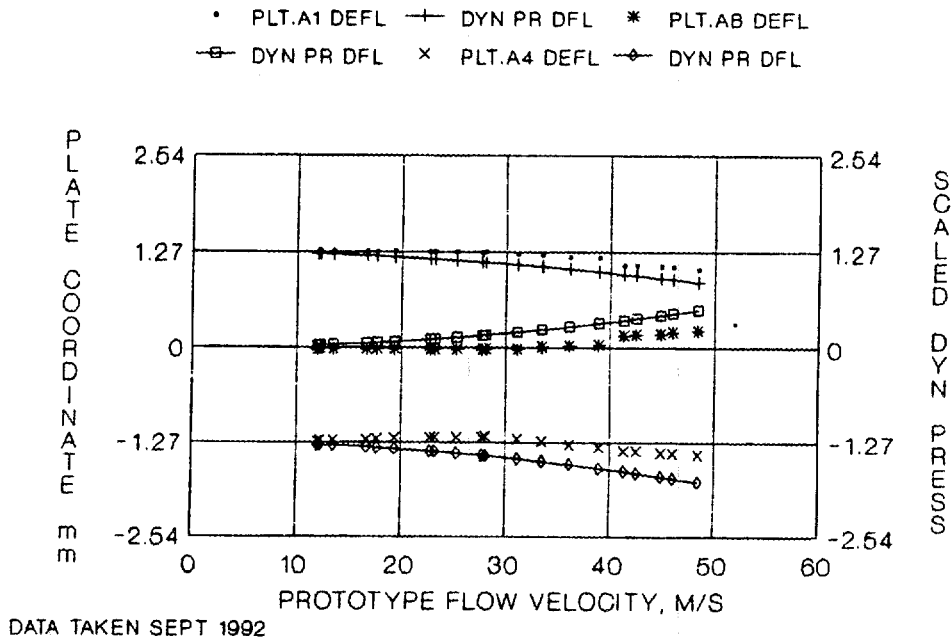


**Fig. 47. Plate A1, A8, A4 three-quarter point dynamic pressure, second model upper ANS plates.**

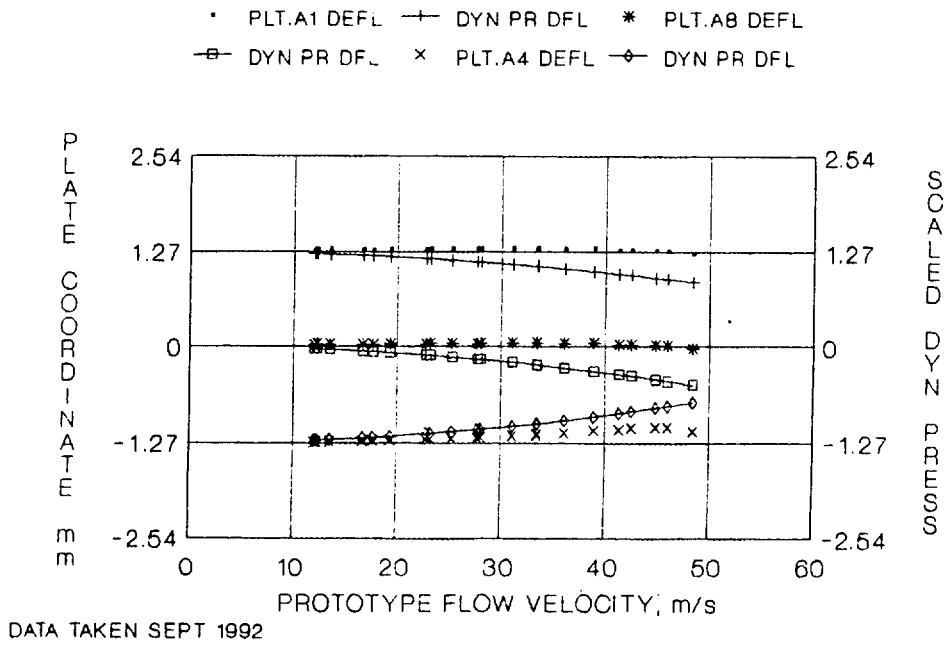


**Fig. 48. Plate A1, A8, A4 exit point dynamic pressure, second model upper ANS plates.**

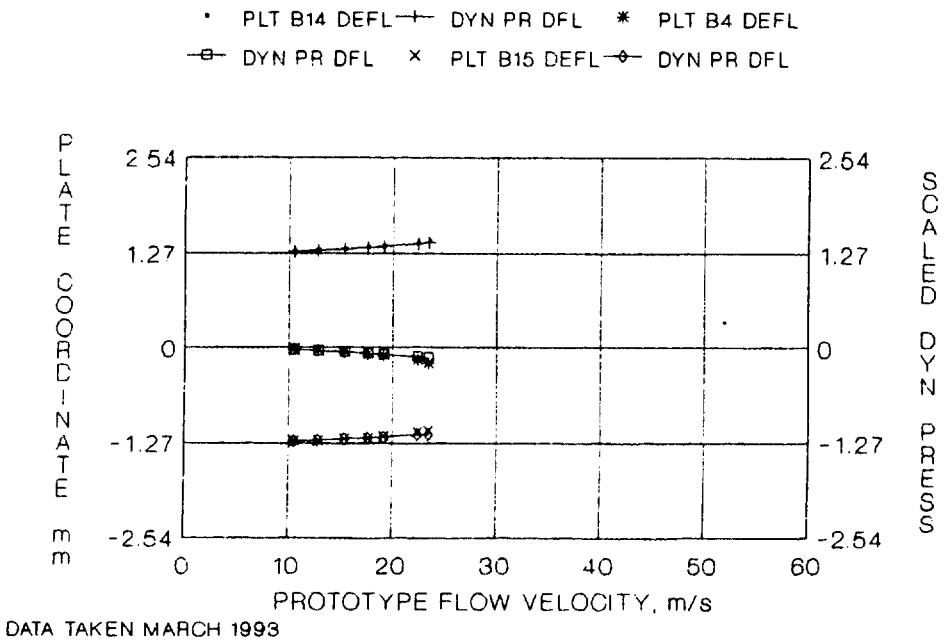


**Fig. 49. Plate B14, B4, B15 entrance dynamic pressure, second model lower ANS plates.**

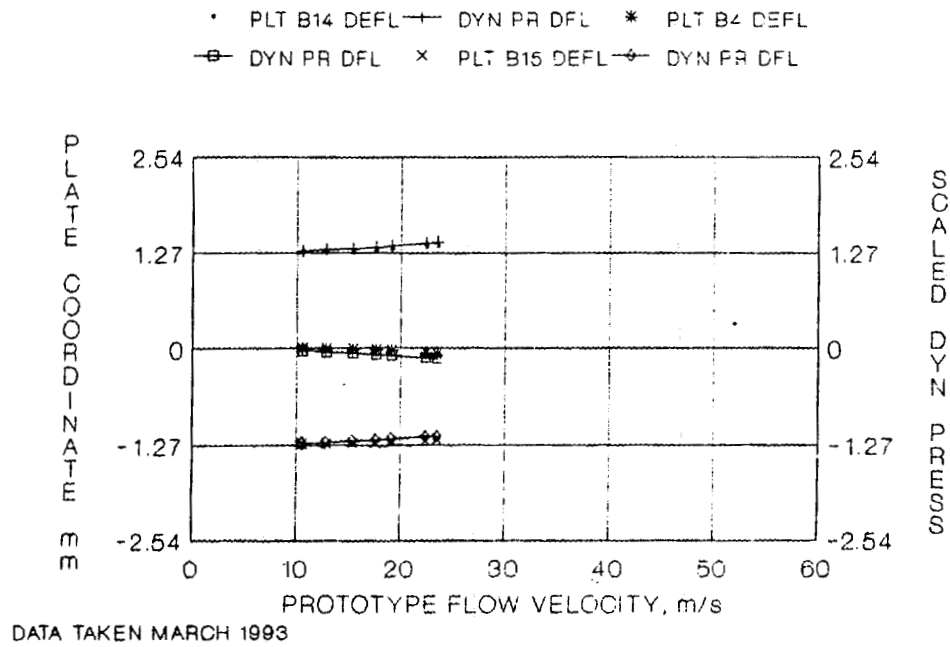


**Fig. 50. Plate B14, B4, B15 quarter point dynamic pressure, second model lower ANS plates.**

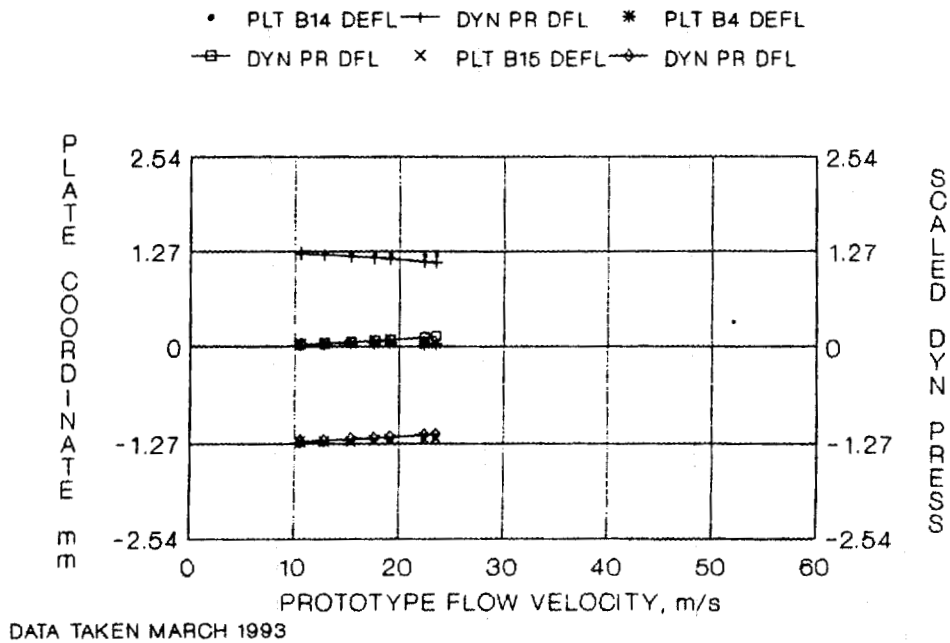


**Fig. 51. Plate B14, B4, B15 half point dynamic pressure, second model lower ANS plates.**

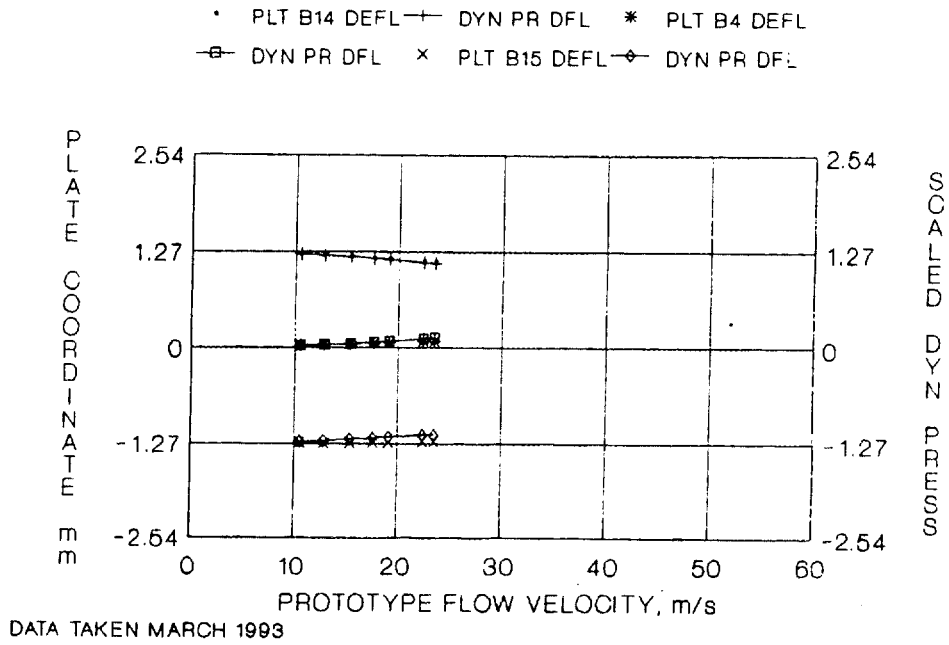


**Fig. 52. Plate B14, B4, B15 three-quarter point dynamic pressure, second model lower ANS plates.**

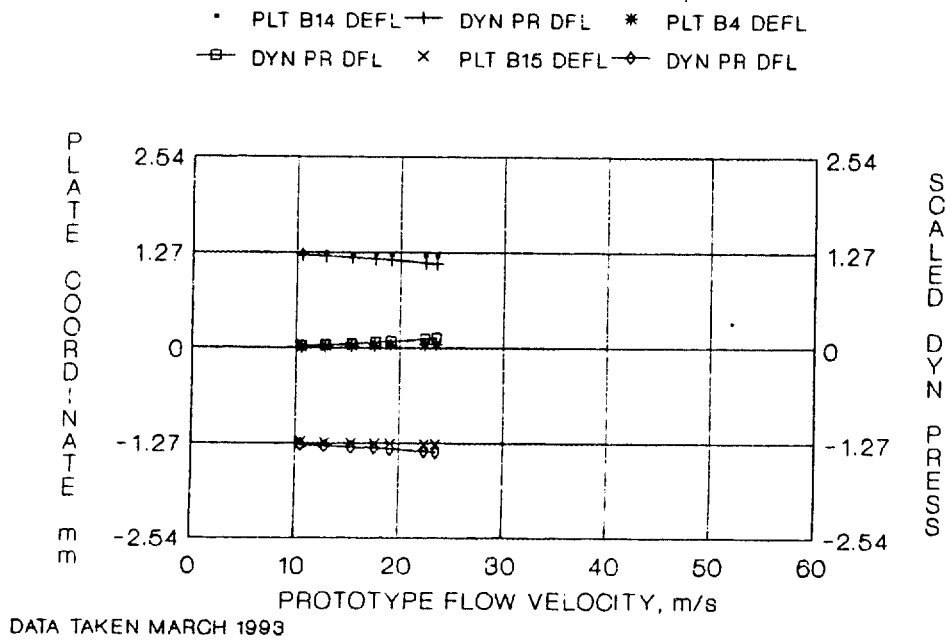


**Fig. 53. Plate B14, B4, B15 exit point dynamic pressure, second model lower ANS plates.**

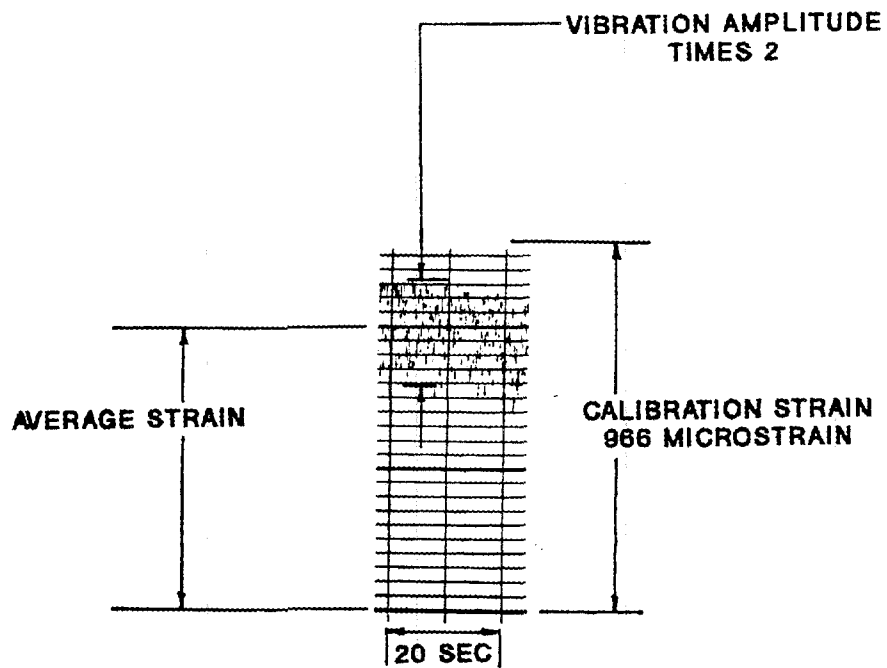


Fig. 54. Plate A4 entrance gage response vs time, flow velocity 33.4 m/s.

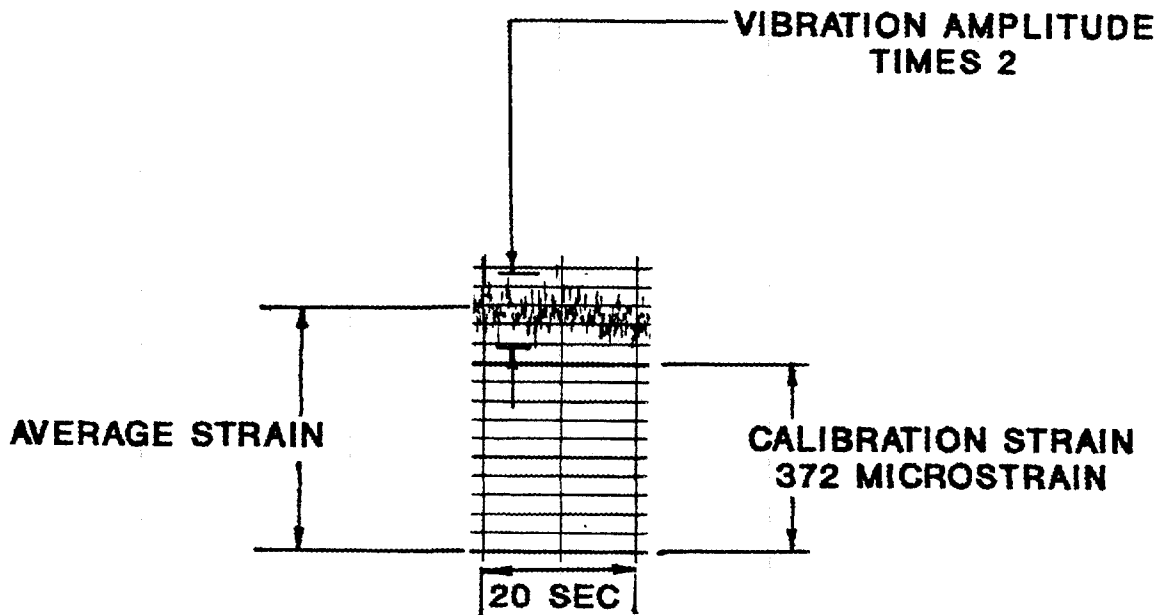
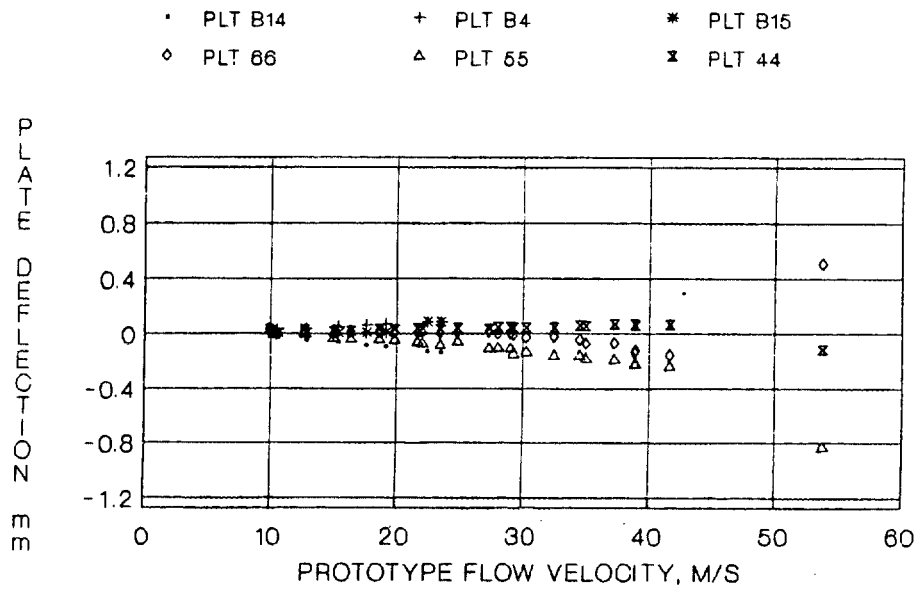
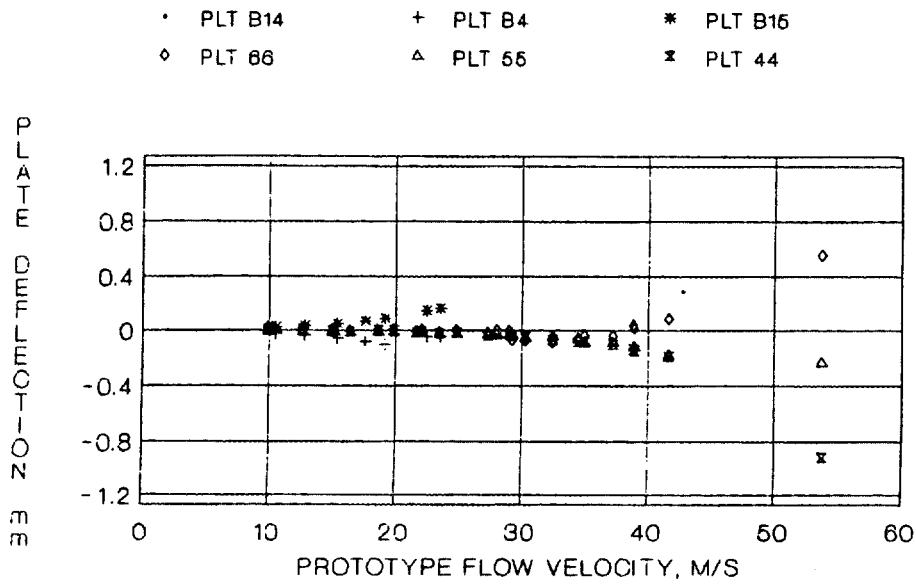


Fig. 55. Plate B4 entrance gage response vs time, flow velocity 23.5 m/s.



**Fig. 56. Lower plate deflection at three-quarter section for comparison of all plates from both test elements.**



**Fig. 57. Lower plate deflection at entrance section for comparison of all plates from both test elements.**

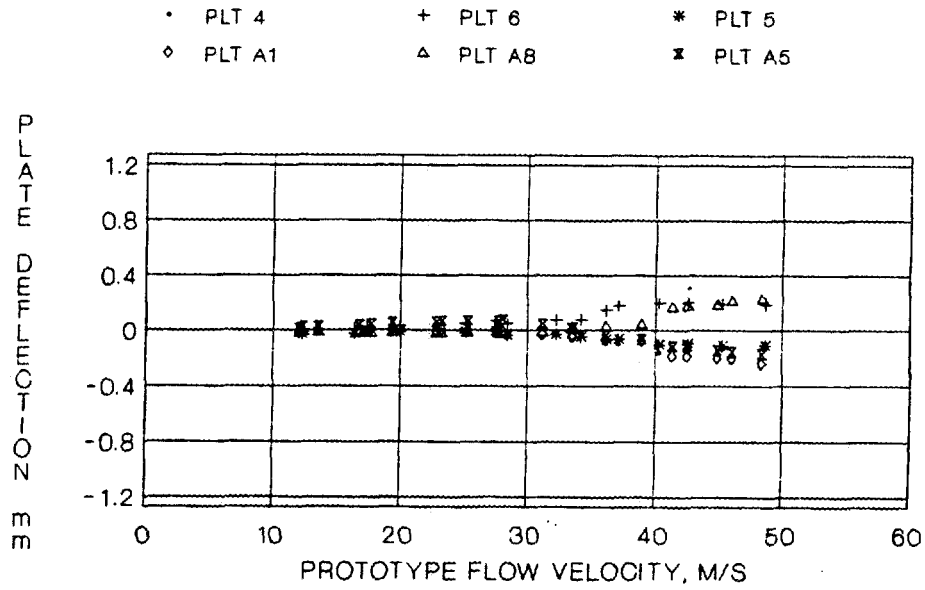


**Fig. 58. Upper plate deflection at three-quarter section for comparison of all plates from both test elements.**

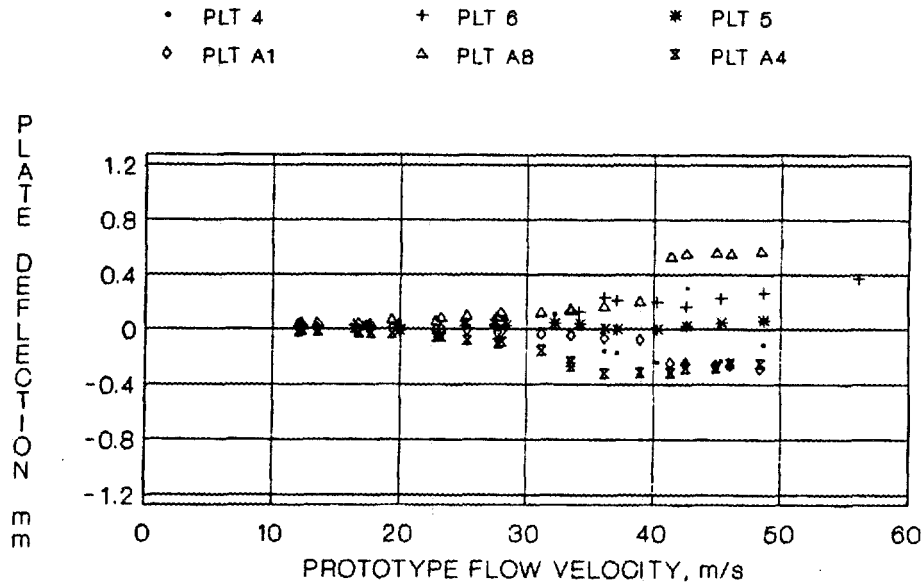


**Fig. 59. Upper plate deflection at entrance section for comparison of all plates from both test elements.**



## 6. DISCUSSION

The separation of the upstream pressure from the pressure drop along the plate channels (Figs. 8–17) gives an indication of the pressure loss in the flow loop because of the flow meter, the 90 degree turn in flow, and the flow straightener (Fig. 4).

The theoretical pressure loss along a flow channel length was calculated using the expression developed from ORNL/TM-12353<sup>1</sup> and is illustrated in Figs. 9–12 and 14–17. The expression does very well in predicting the pressure loss. When the pressure loss is less than the calculated value, the corresponding plate will deflect toward that channel center line. For example, compare the pressure of channel A9–A4 (Fig. 9) with the deflection of plate A4 (Fig. 18). As noted earlier, the average pressures and velocities in the flow channels can be determined reasonably from analytical models. However, the pressure and velocity differences from one channel to an adjacent channel cannot readily be calculated. Unfortunately, this latter information is the information needed to predict the structural response of the plates to coolant flow.

Figures 18–27 illustrate that plate deflection at the planned operating flow of the ANS is small. Note that at the entrance associated with plates A8 and A1, a sudden jump in the plate deflection is observed at an equivalent prototype velocity of 39 m/s (Fig. 18). This effect is rather local as it is not seen at the quarter point (Fig. 19). Channel A8–A1 shows an abrupt pressure jump (Fig. 11) at a model velocity of 8 m/s (this model velocity corresponds to a prototype velocity of 39 m/s). An interpretation of this is that at the 8 m/s model velocity, the entrance flow pattern abruptly changes. Such an occurrence is not uncharacteristic of turbulent flow around objects. This kind of behavior reinforces the suggestion that the upstream flow pattern is a sensitive variable to the channel flow, and, consequently, so is the plate's structural response. At flow velocities above this special value, the channel pressure differential increases slowly until it is again bounded by the dynamic pressure, and deflections again are related to the flow velocity by a smooth function.

There was no experimental evidence of plate collapse as predicted by Sartory's application of Miller's theory to the ANS involute plates (see Figs. 18–22). An opinion as to why a collapse does not occur is noted in the next section.

Generally, the maximum deflection versus the length of the plate is a longitudinal wave form (see Figs. 28–33). The peak deflection did not always occur at the entrance. These characteristics are not predicted by existing analytical plate models.

Figures 34–43 compare the plate deflection with the pressure difference across the plate. The comparison suggests that the strongest variable in causing the plate to deflect is the pressure differential across the plate. The plates can be seen to deflect in almost direct proportion to the differential pressures. Also, it can be observed that the differential pressure is a function of the flow velocity. Since the differential pressure is a function of the flow velocity, the plate deflection must also be a function of the flow velocity. The function relating the differential pressure to the flow velocity is similar to the function relating the dynamic pressure to the flow velocity, although at different magnitudes (see Figs. 44–53). It can be seen that the magnitude of the differential pressure is bounded by the magnitude of the dynamic pressure, with a single exception occurring at the entrance region of plate A8 at a prototype flow velocity of 39 m/s (see Figs. 44–53). The exception is an isolated occurrence, and it is thought that the rotational energy from turbulence available at that entrance point abruptly increases because of a change in the entrance flow pattern. With equal weight given to all of the data, the ability to predict the structural response of the fuel plates is a direct function of the ability to predict the differential pressure across a plate.

The entrance gage on plate A8 (central test plate of the upper element) was connected to a strip chart recorder to monitor the plate response with respect to time. At a prototype flow velocity of 23.2 m/s, a slight resonance was detected in plate A8. The maximum deflection at the entrance to this plate was 0.08 mm. The amplitude of vibration was 0.003 mm with a frequency of about 4 Hz. At a flow velocity of 33.4 m/s, the maximum plate deflection at the entrance increased to 0.14 mm, with an increase in the amplitude of vibration to 0.01 mm at about the same 4 Hz frequency.

Plate A4 (on the convex side of the upper element central plate) had more deflection than plate A8. At a flow velocity of 33.4 m/s, the maximum deflection at the entrance of the plate A4 was 0.24 mm, with an amplitude of oscillation equal to 0.043 mm at 4 Hz. This maximum vibration effect is seen in Fig. 54. At a flow velocity of 36 m/s, the vibration disappeared but began to reappear at 41 m/s flow velocity. The initial magnitude of vibration was small as the vibration returned.

At a flow velocity of 50 m/s through the upper plates, some flutter was evident. The plate would slowly (0.025 Hz) oscillate from a maximum deflection of 0.70 mm to 0.62 mm.

Finally, at a flow velocity of 53.8 m/s, considerable leakage was evident in the upper plate test section, and testing was suspended.

For the lower element test section, the entrance gage of the central plate was monitored with respect to time. The maximum vibrational result is illustrated in Fig. 55. The frequency of vibration for the lower plate models was about 4.4 Hz, which was about 10% higher than the upper plate resonance.

The plate vibrations that were detected occurred at velocities above the ANS operating velocity, and such effects would seemingly not present a problem in the prototype plates. However, relating the vibration results of the model to the vibration results expected in the prototype is not recommended. In developing the scaling factors from model theory for a static or steady-state plate, the inertial properties (mass and acceleration) were not included. Therefore, the model laws developed would not apply to an accelerating plate. When resonance in a plate occurs, if the vibration is small or of a secondary nature, the model laws developed for going from model to prototype will give reasonable results. If the resonance is large or primary, the model laws developed would not be applicable.

Deflection data of the six plates from the upper elements and the six plates from the lower elements are a compilation of data from the first test elements and also from the second test elements (see Figs. 56–59). The variation in the deflection of the plates is an indication of how complicated or how sensitive turbulent flow can be near or at boundaries. The turbulent flow pattern entering the plates is sensitive to factors such as upstream geometry and tolerances, which in turn produce different eddy patterns at the plate entrance. Plate inlet dimensional tolerances also affect the entrance turbulent flow pattern. At the entrance for the upper plates (Fig. 59), plates A4 and A8 bound the plate response; at the three-quarter point (Fig. 58), the bound changes to plates 6 and A1. At the entrance (Fig. 57) for the lower plates, plates 44 and B16 bound the results, and at the three-quarter point (Fig. 56), the bound changes to plates 55 and B16. These variations suggest how complicated the plate response is to the turbulent flow. The ability to calculate this complicated response is limited. Any

conclusions should be based on overall response of the plates and not on any single plate. From these results, it is easy to see the importance of multiple plate tests as opposed to a single plate test.

## 7. CONCLUSIONS

One of the objectives of this experimental effort was to examine the capability of the Sartory model to predict the plate response to coolant flow. In comparing the experimental data in Figs. 18-27 with the calculated collapse velocity from the Sartory model, it is apparent that they do not correlate. An opinion as to why the analytical and the experimental solutions do not correspond is offered.

Before any conclusions are offered, a question that needs some comment is whether or not the experimental data is biased or in error. In reviewing the experimental data, it is noted that in general all of the ANS data are reasonably consistent. This includes data from a single HFIR plate test, two ANS upper plate models each containing five active plates, and two ANS lower plate models each containing five active plates. Plate deflection in all cases was a direct function of the flow velocity, and at a certain flow velocity (above the calculated collapse velocity), flutter was initiated. Only two of the early investigations, Groninger and Kane<sup>12</sup> and Smitsaert,<sup>13</sup> took the flow velocity much past the calculated Miller collapse velocity. These two investigations were consistent with the ANS experimental studies in that plate deflection was a direct function of the flow velocity, and at a certain flow velocity (above the calculated collapse velocity), flutter was initiated. Also, it was determined in experiments that the entrance conditions were sensitive variables in determining the plate response to flow. Essentially, the flow needs to be as smooth entering the plate channels as is reasonable. This also requires that the upstream plate edges be rounded. Since data taken by different investigators on different plates at different times all report similar results, the validity of their results is suggested.

Experimental results and analytical models do not correlate on several points. The data do not show a sudden or rapid increase in the entrance deflection as predicted by analytical models. The most critical deflection region of the plate does not always occur at the entrance as predicted by theory. A longitudinal wave-like deflection, which is not apparent in the analytical models, was observed in all of the experimental tests. The maximum deflection of the plate as determined by experiment is bounded by the dynamic pressure being applied as a load to the plate, whereas the collapse theory predicts unbounded deflection.

Considering the analytical model further, experience has shown that finding an analytical solution involving any turbulent flow is very difficult. For example, the solution to turbulent flow in a pipe is in reality an experimental solution since prior analytical models did not correlate with observations.<sup>2</sup> With the ANS plates, what is desired is the response of the plates to turbulent flow. To determine this response with an analytical model, the boundary conditions on the actual plate surfaces should be accurately described. This includes the surface pressure distribution and the shear stresses, which fluctuate with time and are further complicated in that the fluctuations occur at somewhat random times. Crucial to having a solution for the plate response to flow is the ability to calculate the differences in pressures and shear stresses in the channels that bound the plate. The analytical models do not include the shear stresses as plate boundary conditions, do not include the time dependency of the boundary conditions, do not include eddies, and do not include some important fluid properties such as viscosity. Based on the experiments with the ANS plates, the experiments by other investigators with flat plates, and the experience by all investigators in finding solutions to turbulent flow problems, it appears that an adequate analytical solution for the ANS plates is not yet available.

Relative to a collapse velocity for the ANS plates, it is concluded that a collapse velocity does not occur within a velocity range of more than twice the planned operating flow velocity of the ANS.

A very important observation from the experimental data is that the plate deflection is a function of the pressure difference across the plate, which in turn is a function of the flow velocity. At the operating velocity of the ANS, the maximum plate deflection expected is 6% of the channel opening. It is pointed out that a 6% maximum deflection of the plate does not mean that the channel cross-sectional area decreases by 6%. The plate deflects in an "S" shape from its unloaded involute shape, i.e., part of the plate deflects in one direction and part of the plate deflects in the opposite direction as pressure is applied. Because of this deformed shape, the cross-sectional area changes less than the percentage change of the maximum deflection.

The observation that the plate deflection is a function of the pressure difference is important, because, if the pressure difference can be determined, the plate response can be predicted. Establishing a differential pressure across a plate for design is not straightforward or easy. Sufficient information is not available to analytically determine the pressure

differential across a plate at ANS operating conditions. Experimental data from the involute epoxy plate tests, tests run by other investigators on flat plates, and tests run on the Advanced Test Reactor (Ferris and Moyers),<sup>18</sup> suggest that the differential pressures will be between 50% and 100% of the dynamic pressure. Note that the strain gages on the epoxy involute plates used to signal the maximum plate deflection also show that the strain corresponds to the strain that would occur if a pressure equivalent to one-half the dynamic pressure were applied. If the differential pressures fall in this range at the operating conditions of the ANS plates, some yielding of the plates will occur. The question of whether or not some yielding is a significant problem is appropriate. However, the answer to this question is not straightforward because of unknowns such as stress concentrations at boundaries, thermal effects on material properties, residual stress, and a precise multistress yield theory. An elastic design would allow any extra structural help from yielding to serve as a buffer to alleviate the above cited uncertainties.

Swinson and Yahr<sup>17</sup> observed that the dynamic pressure is an upper bound for the pressure difference across the plate. This observation was true in all of the ANS plate experiments. If the dynamic pressure is used as the design load for the plate, some important conclusions can be made. First, the deflection of the plates at operating flow velocity is not a limitation of the design. This calculated deflection result is also evident from the experimental data. However, it is emphasized that the stresses in the plate do impose a limit. With the plate loaded by the dynamic pressure at the operating ANS flow velocity, stresses on the order of 138 MPa (20,000 psi) are calculated. Aluminum 6061-0 at room temperature has a yield of 55 MPa (8000 psi), a tensile strength of 124 MPa (18,000 psi), and less than these values at increased temperatures. If the differential pressure across a plate equals the magnitude of the dynamic pressure, failure of the involute plates is predicted.

Two recommendations are offered to reduce the stresses in the fuel plates to acceptable levels. One recommendation is to relieve the pressure difference across a plate by connecting the cooling channels. Currently, in fabrication of the HFIR fuel element, grooves are made in the support cylinders for welding the assembly of plates together. If grooves were placed in between the weld grooves but on the opposite side of the support cylinder, the flow channels could be connected. With this arrangement, the coolant would flow through the entire length of the fuel element, and the pressure between channels would be relieved. Ferris and Moyers<sup>18</sup> reported on a technique similar to that proposed here with good success. In their

technique, the vent tubes transferred coolant from the flow channels to a region outside the fuel element; thus, all fluid did not flow the entire length of the fuel plates.

The second recommendation is to substitute a circular arc for the involute plate. The arc would reduce the stresses because of a differential pressure across a plate by a factor of 5. The channel spacing could be held to 1.27 ( $\pm 3\%$ ).

Finally, the conclusions from these tests and analyses are summarized as:

1. The flow in the coolant channels is highly turbulent.
2. An analytical solution is not yet available that will adequately describe the structural response of the fuel plates to coolant flow.
3. An unstable flow collapse velocity does not exist in a prototype flow velocity range from 0 to at least 50 m/s.
4. The maximum plate deflection at the operating flow velocity is 6% of the channel thickness. It is noted that this is not a 6% change in the channel cross-sectional area.
5. Stress in the plate is a more critical design parameter than is the deflection. It is estimated that at the operating flow velocity of the reactor, some stresses in the plates will be above the yield stress for aluminum 6061-0.
6. For design purposes, the structural deformation of the plates can be approximated by assuming the plate is loaded with pressure that is equal to  $0.25 \rho v^2$ .

## 8. REFERENCES

1. W. F. Swinson et al., *Fuel Plate Stability Experiments and Analysis for the Advanced Neutron Source*, ORNL/TM-12353, Martin Marietta Energy Systems, Inc., Oak Ridge Natl. Lab., May 1993.
2. H. Schlichting, *Boundary Layer Theory*, 4th ed., McGraw-Hill Book Company, Inc., New York, 1955.
3. H. Rouse, *Fluid Mechanics for Hydraulic Engineers*, Dover Publications, Inc., New York, 1961.
4. W. K. Stromquist and O. Sisman, *High Flux Reactor Assemblies Vibration and Water Flow*, ORNL-50, Oak Ridge Natl. Lab., June 1948.
5. R. L. Doan, "The Engineering Test Reactor—A Status Report," *Nucleonics* 16, No. 1, 102-105, January 1958.
6. R. G. Beck, E. S. Brown, and J. H. Rainwater, *ETR Core Hydraulics*, IDO-16464, Phillips Petroleum Company, Idaho Operations Office, U.S. Atomic Energy Commission, September 1958.
7. R. G. Beck, *Hydraulics of Modified Fuel Elements for ETR*, IDO-16465, Phillips Petroleum Company, Idaho Operations Office, U.S. Atomic Energy Commission, November 7, 1958.
8. M. H. Bartz and W. C. Francis, *Fuel Element Problems Associated with Operations of the Engineering Test Reactor and Materials Testing Reactor*, TID-7559 (part I), 28-38, U.S. Atomic Energy Commission, August 1959.
9. D. R. Miller, "Critical Flow Velocities for Collapse of Reactor Parallel Plate Fuel Assemblies," *Trans. ASME* 82, 83 (1960).
10. W. L. Zabriskie, *An Experimental Evaluation of the Critical Flow Velocity Formulas for Parallel Plate Assemblies*, Report No. 58GL297, General Electric Company, October 31, 1958.
11. R. V. Simon, *Reactor Technology Report No. 13*, KAPL-2000-10, TID-4500, 15th ed., A.1-A.7, General Electric Company, 1960.
12. R. D. Groninger, and J. J. Kane, "Flow Induced Deflections of Parallel Flat Plates," *Nucl. Sci. Eng.* 16, 218 (1963).
13. G. E. Smissaert, "Static and Dynamic Hydro-Elastic Instabilities in MTR-Type Fuel Elements. Part I. Introduction and Experimental Investigation," *Nucl. Eng. Design* 7, 535-546 (1968).

14. R. C. Gwaltney and C. R. Luttrell, "Critical Flow Velocity for Involute Parallel Fuel Plate Assemblies," *Trans. Am. Nucl. Soc.* **57**, 298 (1988).
15. W. K. Sartory, *Analysis of Hydraulic Instability of ANS Involute Fuel Plates*, ORNL/TM-11580, Martin Marietta Energy Systems, Inc., Oak Ridge Natl. Lab., November 1991.
16. H. Reutler, *Studies of the Stability Behavior of the ILL Fuel Element and Application of the Results to ANS Conditions*, ORNL/TR-88/32, Translated from German, Martin Marietta Energy System, Inc., Oak Ridge Natl. Lab., September 1988.
17. W. F. Swinson and G. T. Yahr, "Dynamic Pressure Approach to Analysis of Reactor Fuel Plate Stability," *Trans. Am. Nucl. Soc.* **61**, 390, June 1990.
18. H. D. Ferris and J. C. Moyers, *Advanced Test Reactor Fuel Element Hydraulic Buckling Tests*, ATR-FE-100 Ca-2, The Babcock and Wilcox Company, Atomic Energy Division, Lynchburg, Virginia, October 1963.

**DISTRIBUTION**

- |                        |                       |                                |
|------------------------|-----------------------|--------------------------------|
| 1. C. W. Alexander     | 35. R. M. Harrington  | 67. S. Raman                   |
| 2. D. J. Alexander     | 36. J. B. Hayter      | 68. C. T. Ramsey               |
| 3. R. R. Allen         | 37. W. R. Hendrich    | 69. J. S. Rayside              |
| 4. E. E. Alston        | 38. S. E. Holliman    | 70. J. P. Renier               |
| 5. J. L. Anderson      | 39. M. M. Houser      | 71. J. B. Roberto              |
| 6. B. R. Appleton      | 40. R. O. Hussung     | 72. M. B. Ruggles              |
| 7. R. L. Battiste      | 41. D. T. Ingersoll   | 73. T. L. Ryan                 |
| 8. R. S. Booth         | 42-45. R. L. Johnson  | 74. D. L. Selby                |
| 9. W. W. Bowman        | 46. J. E. Jones, Jr.  | 75. H. B. Shapira              |
| 10. R. A. Brown        | 47. R. A. Lillie      | 76. M. Siman-Tov               |
| 11. G. W. Bunick       | 48. M. A. Linn        | 77. B. R. Smith                |
| 12-16. J. H. Campbell  | 49. A. T. Lucas       | 78. W. F. Swinson              |
| 17. P. F. Cento        | 50. C. R. Luttrell    | 79. R. P. Taleyarkhan          |
| 18. N. C. J. Chen      | 51. M. F. Marchbanks  | 80. D. W. Thiesen              |
| 19. K. K. Chipley      | 52. J. A. March-Leuba | 81. P. B. Thompson             |
| 20. J. E. Cleaves      | 53. B. S. Maxon       | 82. K. R. Thoms                |
| 21. J. T. Cleveland    | 54. G. T. Mays        | 83. S. R. Tompkins             |
| 22. J. A. Clinard      | 55. S. V. McGrath     | 84. B. D. Warnick              |
| 23. G. L. Copeland     | 56. T. J. McManamy    | 85. C. D. West                 |
| 24. B. L. Corbett      | 57. G. R. McNutt      | 86. J. L. Westbrook            |
| 25. J. M. Corum        | 58. J. T. Michalczo   | 87. D. M. Williams             |
| 26. J. R. Dixon        | 59. R. M. Moon        | 88. B. A. Worley               |
| 27. F. F. Dyer         | 60. D. G. Morris      | 89. G. T. Yahr                 |
| 28. K. Farrell         | 61. D. L. Moses       | 90. G. L. Yoder                |
| 29. D. K. Felde        | 62. R. E. Pawel       | 91. ORNL Patent Section        |
| 30. R. E. Fenstermaker | 63. H. R. Payne       | 92-93. Document Res. Library   |
| 31. M. L. Gildner      | 64. F. J. Peretz      | 94. Y-12 Technical Library     |
| 32. R. G. Gilliland    | 65. A. B. Poole       | 95. Laboratory Records Dept.   |
| 33. H. A. Glover       | 66. C. C. Queen       | 96-97. Laboratory Records (RC) |
| 34. R. C. Gwaltney     |                       |                                |

**EXTERNAL DISTRIBUTION**

98. R. Awan, U.S. Department of Energy, NE-473, Washington, DC 20585.
99. K. K. Conway, Laboratory Facilities Branch, U.S. Department of Energy, Oak Ridge Operations Office, CE-523, P.O. Box 2001, Oak Ridge, TN 37831-2001.
100. R. R. Fullwood, Bldg. 130, Brookhaven National Laboratory, Upton, NY 11973.
101. R. Gambill, Route 5, Box 220, Clinton, TN 37716.
102. A. F. Henry, Professor, Department of Nuclear Engineering, Massachusetts Institute of Technology, 77 Massachusetts Avenue, Cambridge, MA 02139.
103. R. A. Hunter, Director, Office of Facilities, Fuel Cycle, and Test Programs, Nuclear Energy Division, U.S. Department of Energy, NE-47, Washington, DC 20585.

104. L. C. Ianniello, Acting Associate Director, Office of Basic Energy Sciences, Office of Energy Research, U.S. Department of Energy, ER-10, Washington, DC 20585.
105. T. L. Kerlin, University of Tennessee, College of Engineering, 315 Pasqua Engineering Building, Knoxville, TN 37996-2300.
106. J. A. Lake, Manager, Nuclear Engineering and Reactor Design, Idaho National Engineering Laboratory, P.O. Box 1625, Idaho Falls, ID 83415.
107. J. E. Mays, Research and Test Reactor Fuel Elements, Babcock and Wilcox Co., P.O. Box 785, Lynchburg, VA 24505.
108. J. P. Mulkey, Division of Energy Research Reactors, Office of Nuclear Energy, U.S. Department of Energy, NE-473, Washington, DC 20585.
109. W. T. Oosterhuis, Materials Sciences Division, Office of Basic Energy Sciences, Office of Energy Research, U.S. Department of Energy, ER-132, Washington, DC 20585.
110. H. Reutler, Siemens, Friedrich—Ebert Strasse, D-5060 Bergish, Gladbach-1, Germany.
111. J. M. Ryskamp, Idaho National Engineering Laboratory, P.O. Box 1625, Idaho Falls, ID 83415-3885.
112. J. L. Snelgrove, Coordinator, Engineering Applications, RERTR Program, Argonne National Laboratory, 9700 South Cass Avenue, Argonne, IL 60439.
113. I. Thomas, Director, Materials Science Division, Office of Energy Research, U.S. Department of Energy, ER-13, Washington, DC 20585.
- 114–119. U.S. Department of Energy, ANS Project Office, Oak Ridge Operations Office, FEDC, MS-8218, P.O. Box 2009, Oak Ridge, TN 37831-8218.
120. H. G. Wood, III, Associate Professor, Department of Mechanical and Aerospace Engineering, Thornton Hall, University of Virginia, Charlottesville, VA 22901.
121. Office of Assistant Manager for Energy Research and Development, U.S. Department of Energy, Oak Ridge Operations Office, P.O. Box 2001, Oak Ridge, TN 37831.
- 122–123. Office of Scientific and Technical Information, P.O. Box 62, Oak Ridge, TN 37831.